Rapid communication: Nonlinear sensitivity of El Niño-Southern Oscillation across climate states

Gabriel M. Pontes[1,2]*, Pedro L. Silva Dias[3] & Laurie Menviel[1,2]

Affiliations:

[1] Climate Change Research Centre, University of New South Wales, Sydney, NSW, Australia

[2] Australian Centre for Excellence in Antarctic Sciences, University of New South Wales, Sydney, NSW, Australia

[3] Institute of Astronomy, Geophysics and Atmospheric Sciences, University of São Paulo, São Paulo, SP, Brazil

*Corresponding author e-mail: g.pontes@unsw.edu.au.

Abstract

The El Niño-Southern Oscillation (ENSO) is the dominant mode of tropical climate variability. Understanding its sensitivity to climate states is of societal and ecosystem importance given the unabated global warming. Paleoclimate archives and climate models suggest that ENSO activity depends on mean state conditions. However, due to climate model biases, short. observational record and proxy-data uncertainties, evaluating ENSO sensitivity remains challenging. Here we combine ~~state-of-the-art~~climate model simulations of past climates and future warming, performed under the Paleoclimate and Coupled Model Intercomparison Projects (PMIP and CMIP, respectively), to evaluate ENSO activity throughout a wide range of climate states. We find that the sensitivity of ENSO to the background climate is nonlinear and tied to the climatological position of the Intertropical and South Pacific ~~tropical Pacific convection centers, namely the Intertropical and South Pacific~~ Convergence Zones. Simulations with atmospheric CO_2 lower than today display a poleward shift of the convection centers and weakened ENSO. Moderate equatorward shifts of the convection centers occur under CO_2-induced warming increasing ENSO activity, while strong equatorward shifts reduce ENSO variability in extreme CO_2 warming scenarios, resulting in a permanent El Niño-like mean state. Furthermore, we find that Eastern Pacific El Niño~~s~~ ~~are~~ is more sensitive to the background state than Central El Niño events. Our results provide a comprehensive mechanism of how tropical Pacific mean state modulates ENSO activity.

1. Introduction

The El Niño-Southern Oscillation (ENSO) is a coupled ocean-atmosphere zonal oscillation sourced in the equatorial Pacific that results in either higher (El Niño) or lower (La Niña) sea surface temperatures (SST) in the central and eastern Pacific, with strong impacts worldwide (Ropelewski & Halpert, 1987). For this reason, the scientific community has concentrated efforts in identifying changes in ENSO variability and their drivers in past climates and future projections (Cai et al., 2021; Ford et al., 2015; Pontes et al., 2022b; Thirumalai et al., 2024; White and Ravelo, 2020).

~~At ~3.3 million years (Ma), greatly reduced water-mass transport through the Indonesian and Panamá seaways due to tectonic changes (De Schepper et al., 2014) likely set up conditions for the full development of ENSO, which has been the most important driver of year-to-year climate variability during the instrumental period. Before that time, during the early Pliocene (~4-5 million years ago [Ma]), it is likely the necessary conditions for ENSO development in the equatorial Pacific Ocean were not present due to zonal advection across both zonal boundaries (De Schepper et al., 2014), the absence of a strong zonal SST gradient (Fedorov et al., 2015; White & Ravelo, 2020) and a Pacific Walker cell extending to the Indian Ocean (van der Lubbe et al., 2021). While proxy-data and modelling studies provide evidence of varying ENSO activity over the last 3.3 Ma, due to changes in thermocline (Ford et al., 2015; White & Ravelo, 2020), zonal SST gradient (Sadekov et al., 2013), Walker cell extent (Pausata et al., 2017), Inter-Tropical Convergence Zone (ITCZ) position (Pontes et al., 2022), among others (Z. Liu, 2002; Tudhope et al., 2001), a common mechanism explaining such ENSO behavior is hitherto missing.~~

The past 3.3 Ma encompass three key periods that have been extensively studied as they can improve~~under intense investigation due to their importance in improving~~ our understanding of climate dynamics and help constrain future projections (Burke et al., 2018; Thirumalai et al., 2024)~~during warm states~~. First, t~~T~~he mid-Pliocene warm period (referred as mid-Pliocene,

~3,200 thousand years ago (ka)~~~3.2 Ma~~) featured a global mean temperature 2-4ºC higher than pre-industrial (PI) and elevated atmospheric CO2 concentrations (~400 ppmv) (Lunt et al., 2012). Over this period, proxy-data do not provide a clear picture on ENSO changes and suggest the important role of the sensitivity of the equatorial thermocline in maintaining ENSO activity (Watanabe et al., 2011; White & Ravelo, 2020).~~,~~ C~~ but c~~limate models, however, systematically indicate reduced variability driven by a northward shift of the Intertropical Convergence Zone (ITCZ) (Pontes et al., 2022). Other periods of interest are the Last Interglacial period (LIG, ~129 116 thousand years ago [ka]), which was the warmest interglacial of the last 800 ka (PAGES working Group~~Berger et al.~~, 2016), and the mid-Holocene thermal maximum (MH ~8–4 ka). During both ~~interglacials~~LIG and MH, atmospheric CO_2 concentrations were~~as~~ slightly lower than pre-industrial (PI) levels but ~~with higher~~ boreal summer insolation in the Northern Hemisphere was higher (up to 70 $W.m^{-2}$ and 25 $W.m^{-2}$, respectively). For both ~~the LIG and the mid-Holocene~~periods, most proxy and models agree on reduced ENSO activity (J. Brown et al., 2020; Emile-Geay et al., 2016), possibly related to weaker thermocline feedback (Chen et al., 2019), amplified by a stronger Walker circulation (Pausata et al., 2017).~~ ~~ Lastly, during the Last Glacial Maximum (LGM, ~21ka) when CO_2 concentrations were ~190 ppmv (Marcott et al., 2014), a deeper equatorial mixed-layer has been suggested to drive reduced ENSO variability (Ford et al., 2015; Thirumalai et al., 2024).

While paleo modelling studies of past warm climates suggest reduced ENSO variability, future projections suggest~~under a future high-emissions scenario models tend to simulate~~ enhanced ENSO under anthropogenic warming for ~~during~~ the 21st century (Cai et al., 2018). Nevertheless, extended simulations of the high-emissions scenario (SSP5-8.5) until 2300 and equilibrated long-term (over 1,000 years) CO2-driven simulations (e.g., abrupt 4- and 8-times CO2) under the Long Run Model Intercomparison Project (LongRunMIP), show a robust decrease in ENSO (Callahan et al., 2021; Peng et al., 2024; Zheng et al., 2022). ENSO decline under these scenarios has been attributed to collapsed eastern Pacific upwelling and weakened zonal SST gradient. ~~Here, to investigate the effect of changes in Pacific mean state on ENSO~~

~~variability, we analyze ENSO activity within the 4th phase of Paleoclimate and 6th phase of the Coupled Model Intercomparison Projects (PMIP4 and CMIP6, respectively).~~

Studies of specific time slices and scenarios led to significant advancements in the understanding of ENSO's dynamical processes. These studies usually suggest that changes in the equatorial Pacific mean state (e.g., upwelling, zonal SST gradient and ITCZ) are responsible for changing ENSO activity, thus contributing to the hypothesis that ENSO is modulated by the background state. Under this hypothesis, a strong mean circulation (i.e. La Niña-like mean state) inhibits the development of wind and SST anomalies, effectively suppressing ENSO variability, while a weak mean circulation (i.e. El Niño like mean state) favors the development of anomalies that can lead to ENSO events. However, the evaluation of a single scenario provides a limited view of the broader ENSO response across climate states. To comprehensively evaluate whether and how ENSO activity can be modulated by the mean state a consistent framework that covers a wide range of background states is needed. In this context, we combine climate model output from the Coupled and Paleoclimate Modelling Intercomparison Projects phases 6 (CMIP6) and 4 (PMIP4), covering seven different scenarios, to investigate the role of the Pacific Ocean mean state in modulating ENSO variability.

2. Data and Methods

~~The PMIP4 project aims to gather the modelling community to consistently simulate key past periods in Earth's history.~~ Here, we analyze four~~3~~ climate scenarios part of PMIP4: the mid-Pliocene (3.2 Ma, CO2=400ppm; Haywood et al., 2020), Last-interglacial (LIG, 127ka, CO2=275ppm, Otto-Bliesner et al., 2021), and mid-Holocene (MH, 6ka, CO2=285ppm, Brierley et al., 2020) and the Last Glacial Maximum (LGM; 21ka; Kageyama et al., 2021). In addition, we incorporate in our extended future projections of the high- (SSP5-8.5) and low-emissions (SSP1-2.6) scenarios (O'neill et al., 2016). In SSP5-8.5, anthropogenic radiative forcing continues to increase beyond the year 2100, reaching a level of ~12 W m^{-2} in 2250 and stabilizing afterwards. In SSP1-2.6, radiative forcing reaches 2.6 W m^{-2} in 2100 and then slowly declines, stabilizing at around 2.0 W m^{-2} onwards from 2200~~analysis projections for the 21st~~

~~century under a high-emissions scenario (ssp585, CO2=400 to 1135 ppm,O'neill et al., 2016).~~ Finally, we also include the hypothetical ~~and~~ the hypothetical scenario that abruptly increases atmospheric CO2 to four times pre-industrial levels (Supplementary Information Table S1). This data totalizes 83 simulations covering 7 different scenarios (Supplementary Table S1). We use each model's~~the~~ pre-industrial control simulation (PI, CO2=284 ppm~~; PI~~) simulations as reference for all scenarios. For all paleoclimate experiments (including abrupt4xCO2 and piControl) we use the last 100 years of each model's simulation. For the future scenarios, SSP5-8.5 and SSP1-2.6, we use the time slice from year 2251 to 2300 (referred to as SSP585-23 and SSP126-23, respectively) as representative of a near-equilibrium state.

Given that ENSO is a complex phenomenon of ocean-atmosphere interaction, not all climate models accurately simulate key processes of ENSO dynamics, resulting in poor ENSO simulations. To avoid being misled by results from models that do not capture ENSO dynamics properly, we apply a selection criterium based on the nonlinear convective feedback, which contributes to the observed positive skewness of SST anomalies in the eastern Pacific (Appendix Text A1) (Dommenget et al., 2012). Here, we use data from the Global Precipitation Climatology Project and the Hadley Centre Sea Surface Temperature datasets to calculate the strength of this feedback in observations. This results in 61 selected simulations of past climates and future scenarios (Supplementary Information Table S1). ~~To account for ENSO complexity, ENSO variability is decomposed into two types: C-index (Central Pacific; CP-ENSO), E-index (eastern Pacific; EP-ENSO; Takahashi et al., 2011), which have distinct anomalies centers in the equatorial Pacific and distinct impacts on remote areas. CP-ENSO variability is characterized by low intensity warming in the central- western Pacific, while EP-ENSO events are recognized by strong warming in the central-~~

~~eastern Pacific. As here we evaluate ENSO dynamics in climate models, the simulated anomaly centers of CP and EP-ENSO may vary across models. As such, C and E indices are obtained through combining the first two Empirical Orthogonal Functions of SST anomalies in tropical Pacific (15ºS-15ºN; 140ºE-80ºW). SST anomalies are computed by removing the monthly annual cycle. The first two principal components time series are combined to obtain the E ((PC1-PC2)/√2) and C ((PC1+PC2)/√2) indices (Supporting Information Fig. S1). SSTs of the ssp585 scenario are quadratically detrended before applying the EOF analysis. For completeness, we also evaluate SST variability in the Niño3 region (5ºS-5ºN; 150ºW-90ºW), which is projected approximately 45º between CP and EP-ENSO axes in the EOF space.~~

We use ~~Finally,~~ the standard deviation of the of SST anomalies in the Niño3 region (5ºS-5ºN; 150ºW-90ºW) as a measure~~time series of all indices are used as a proxy~~ of ENSO amplitude (Taschetto et al., 2014).

Lastly, we evaluate the nonlinear ENSO sensitivity to the background state through the nonlinear coefficient (a) of the quadratic regression model ($y(x) = ax^2 + bx + g$), while the precision of the nonlinear relationship is assessed through the coefficient of determination (R^2). ~~Given that ENSO is a complex phenomenon of ocean-atmosphere interaction, not all climate models accurately simulate key processes of ENSO dynamics, resulting in poor ENSO simulations. To avoid being misleaded by results from models that do not capture ENSO dynamics, we apply two selection criteria based on the nonlinear Bjerknes feedback and nonlinear convective feedback, both of which contribute to the observed positive skewness of SST anomalies in the eastern Pacific (Appendix A and Supplementary Information Figure S2) (Cai et al., 2018; Dommenget et al., 2012). Applying these criteria results in 34 selected simulations of past climates and future scenarios out of the initial 87 simulations (excluding their respective PI simulations; Supporting information Tables S1 and S2).~~

3. Results

3.1 Mean state changes and ENSO activity

All three past warm climates (mid-Holocene, Last-interglacial and mid-Pliocene) share similar conditions in the tropical Pacific Ocean, though for different reasons (Brierley et al., 2020; Otto-Bliesner et al., 2021; Pontes et al., 2020). Firstly, the ITCZ shifts northward in all warm paleoclimate scenarios considered due to increased difference in inter-hemispheric warming. In the mid-Pliocene simulations, this is attributed to enhanced albedo feedback in the Northern Hemisphere due to large sea-ice and land ice losses and enhanced vegetation area, while increased insolation in the Northern Hemisphere is the main driver in the MH and LIG (Brierley et al., 2020; Otto-Bliesner et al., 2021; Pontes et al., 2020). An ITCZ displaced northward allows~~Firstly, they are characterized by~~ intensified equatorial trade winds~~,~~ ~~especially~~ in the central-western Pacific (Fig. 1a-c), which ~~. Intensified trades~~ cause SSTs to be lower in the equatorial Pacific than in the surrounding area due to the Wind-Evaporation-SST (WES) feedback (Vimont et al., 2001)~~(Figure 1a-c),~~ ~~and~~ thus strengthening the~~ed~~ equatorial upwelling. Such climatic anomalies resemble a La Niña-like mean state, associated with reduced ENSO variability (Fig. 1g and Supplementary Table S1).~~Secondly, the increased difference in inter-hemispheric warming leads to a northward shift of the ITCZ (Supporting Information Fig. S3). In contrast, the anthropogenic warming scenario (ssp585) shows an equatorially amplified warming with weakened trades and upwelling, conditions which are similar to that of El Niño events (Figure 1d). In these simulations, equatorially enhanced warming shifts the Pacific ITCZ and the South Pacific Convergence Zone (SPCZ) equatorward (Mamalakis et al., 2021; Supporting Information Fig. S3).~~

In contrast, CO2-driven scenarios (SSP126-23, SSP585-23 and abrupt4xCO2) resemble an El Niño-like mean state (Figure 1d). It is interesting to note that as the SST warming intensifies, both the ITCZ and Subtropical Pacific Convergence Zone (SPCZ) tend to move equatorward (Fig. 1d-f), progressively weakening the equatorial trades and eastern upwelling. In moderate CO_2-driven warming scenarios (e.g., SSP126-23) these changes allow enhanced ENSO variability (Fig. 1g). Interestingly, however, ENSO variability tends to decrease under

strong warming scenarios (e.g., SSP585-23), when the ITCZ and SPCZ are nearly collapsed at the equator (Fig. 1e-g), thus resulting in a nonlinear ENSO response to the background state. As the position of the convergence zones can be directly modulated by changes in the atmospheric meridional heat transport (Pontes et al., 2020; Schneider et al., 2014), which provides a linkage between equatorial Pacific and large-scale changes (e.g., orbital forcing and ice sheets), we use them as a proxy for changes in the tropical Pacific mean state. ~~The response of ENSO in PMIP4 and CMIP6 simulations is likely tied to its mean state. Simulations of past warm periods show a near-unanimous weakening of ENSO variability and a more La Niña-like mean state, while the ssp585 simulations tend to show an increased ENSO variability with a more El Niño-like mean state (Figure 1e; all values computed in this study can be found in Supporting Information Table S1). In this context, studies have hypothesized that the strength of the coupled atmosphere-ocean climatological circulation can modulate ENSO variability (Pontes et al., 2022; Santoso et al., 2013), since, by definition, ENSO is a deviation from the mean climate.~~

3.2 Role of tropical convection centers

To evaluate the effect of the position of the Convergence Zones on ENSO activity we develop an index that captures their combined displacement during the developing and mature ENSO phases (austral spring and summer) (Pontes et al., 2022a). The ITCZ and SPCZ positions are computed as the precipitation weighted average over latitudes in which precipitation is greater than 70% of the maximum zonally averaged precipitation in each hemisphere (0º-20ºN and 20ºS-0º, respectively). This methodology captures migrations of the ITCZ and the SPCZ independently from one another. As our objective is to quantify their overall displacement relative to the equator (e.g., equatorward shit of the ITCZ and SPCZ represent an El Niño-like mean state), we consider their absolute values. The index D is obtained through quantifying their combined displacement relative to the model's piControl position:

$$D = [|ITCZ_S| - |ITCZ_{PI}|] + [|SPCZ_S| - |SPCZ_{PI}|]$$

where the subscript 'S' indicates the position of the ITCZ and SPCZ in the perturbation

scenarios and the subscript 'PI' denotes their position in their respective pre-industrial simulation. Hereafter, the index D is referred to as the convection-centers index and is, by definition, positive for poleward displacements of the Convergence Zones. It is important noting that in all scenarios the Pacific ITCZ lies in the Northern Hemisphere, therefore a poleward movement reflects a northward shift, whereas for the SPCZ, a poleward displacement reflects a southward shift.

It is important noting that double-ITCZ biases may affect the calculated SPCZ position. The double-ITCZ bias is an artificial feature produced by most climate models that overestimates the tropical precipitation south of the equator in the central-eastern Pacific. This biased precipitation artificially induces the index D to capture an apparent SPCZ displaced northwards. Nevertheless, although being an artificial feature, the double-ITCZ dynamically influences the tropical Pacific climate through simulating weaker trade winds and warmer SSTs than in observations and therefore affecting the model's ENSO response. We thus do not differentiate between the southern branch of the double ITCZ and the SPCZ in our evaluation.

~~Important features that can modulate the strength of the coupled climatological circulation in the equatorial Pacific are the position of the atmospheric convection centers. There are two main convection centers in the tropical Pacific, the ITCZ and the SPCZ, whose meridional positions affect ENSO dynamics. Firstly, the more distant the convection centers are from the equator the reduced is ENSO growth and occurrence of extreme rainfall events (Pontes et al., 2022). Furthermore, the positions of the convection centers are key to determining the equatorial wind field and the associated ocean response. Convective regions are characterized by a convergent horizontal wind field, where horizontal wind velocities tend to zero at their centers. Away from convective regions winds are more intense due to increased horizontal pressure gradients. Thus, the position of the convection centers determines the momentum transfer from the atmosphere to the ocean that could impact oceanic stratification and thermocline slope in the equatorial Pacific. These processes ultimately influence the~~

~~effectiveness of the dynamical ocean-atmosphere coupling, important for ENSO development (Jin et al., 2006). For instance, a northward ITCZ displacement was found to be the main driver of reduced ENSO activity in the mid-Pliocene (Pontes et al., 2022), has modulated ENSO on a multidecadal timescale over the past 40 years (Hu & Fedorov, 2018) and is responsible for ENSO hysteresis under CO2 removal scenarios (C. Liu et al., 2023). Finally, idealized experiments of changes in extratropical meridional SST gradients in the Pacific Ocean, which affect the ITCZ position, consistently impact ENSO activity (Chiang et al., 2008).~~

We find that the ENSO-convection centers relationship is nonlinear (Fig. 2 and Supplementary Table S1). ~~To evaluate the effect of the position of the convection centers on ENSO activity, the combined meridional displacement of the ITCZ and SPCZ is tracked during the developing and mature ENSO phases (austral spring-summer; Supporting Information Text T2). A preliminary result, which includes all models and simulations, indicates that the ENSO- convection centers relationship exhibits a quadratic shape ($R2 = 0.35 \pm 0.01$; Appendix B).~~ This relationship indicates that there are two mean states that tend to inhibit ENSO development and there is an optimal distance at which the convection centers must be from the equator to maximize ENSO variability. Overall, poleward ($D>0^{o}$)~~shifts~~ and strong ($D<-8^{o}$)~~(>8º; combined absolute ITCZ and SPCZ meridional displacement)~~ equatorward shifts of the convection centers, relative to their position in the PI climate, are associated with reduced ENSO variability, whereas moderate ~~(<8º)~~ equatorward shifts ($-8^{o}<D<0^{o}$) ~~increase~~ enhance ENSO activity. Analysis of how this relationship affects Central and Eastern Pacific ENSO types and the 21st century transient ENSO response are included in the Appendix Text A2. ~~Applying the model selection criteria (see section 2) results in a further significant relationship that holds across different types of ENSO and metrics (Figure 2; further details and sensitivity tests are shown in Supporting Information Text T3 and Fig. S4).~~

~~The ENSO-convection centers relationship reveals important differences between CP- and EP-ENSO types. First, CP-ENSO activity is likely less sensitive to changes in the~~

~~meanstate as indicated by a wider shape of the quadratic fit (a= 0.87, where a is the nonlinear coefficient of the quadratic model: $y(x) = ax^2 + bx + g$) and weaker relationship (R^2 = 0.40) compared to EP-ENSO (a = -2.18; R^2 = 0.75). Additionally, in our subset of models, CP-ENSO variability shows a non-robust increase under the ssp585 scenario (60% model agreement, Figure 2a). Nonetheless, if selecting models based only on the nonlinear Bjerknes feedback criteria, CP-ENSO show significantly increased variability (70% model agreement; Table S1 and S2), consistent with a previous study (Shin et al., 2022). The CP-ENSO sensitivity to different criteria may help explain inconsistent findings in previous CMIP phases (Cai et al., 2018; Taschetto et al., 2014).~~

~~On the other hand, EP-ENSO is strongly modulated by the position of the convection centers (R^2 = 0.75) and exhibits a high sensitivity to climate states (a = -2.18; Figure 2d). According to this finding, the climate system supports a maximum increase in EP-ENSO variance of approximately 47%, which is achieved with an overall equatorward displacement in the position of the convection centers of ~4.7º (Figure 2b). Finally, the Niño3 index likely captures a combination of CP and EP-ENSO variabilities (R^2 = 0.65, a = -1.47; Figure 2c) since its region encompasses both CP and EP anomalies (Takahashi et al., 2011).~~

~~3.3 3-D view of ENSO dynamics~~

———In exploring the causes of the nonlinear ENSO sensitivity to background state, we find that the position of the Convergence Zones modulates both atmospheric and oceanic processes important for ENSO development~~both atmospheric and oceanic processes play an important role in explaining the ENSO- convection centers relationship~~. First, we investigate the rainfall response to the convection centers migration through evaluating ~~To investigate the effect of the position of the convection centers over convective anomalies, we first evaluate~~ the frequency of extreme rainfall events (>5 mm.day^{-1}) in the eastern Pacific (Niño3 region) associated with the displacement of the ~~convection centers~~Convergence Zones (Fig.~~ure~~ 3a). We find that poleward shifts of the convection centers reduce the frequency of extreme events

from one event 15.3±7.5~~per 9.4±3.6~~ years in ~~the~~ PI ~~control~~ to one event per 26.9±18.3 ~~15.6±9.6~~ years, indicating suppressed convective feedback (Fig~~ure~~ 3a). The convective feedback is further suppressed as the ITCZ shifts northwards until a full La Niña-like mean state is reached and no extreme El Niño events occur~~—~~, which is illustrated by the CCSM4-UTRECTH mid-Pliocene simulation (Fig. 3a; Supplementary Table S1)~~(Pontes et al., 2022)~~. Moderate equatorward shifts of the convection centers allow a more intense convective feedback and increase the frequency of extreme events (one event per 2.9±0.4 years; Fig. 3a)~~to one event per 2.6±0.3 years (Figure 3a)~~. This is consistent with studies that suggested that as ENSO's frequency approaches the annual cycle frequency (represent here by one event per year), ENSO variability tends to increase (Timmermann2007; Liu2002), a process known as 'ENSO frequency entrainment'. Strong equatorward displacements of the convection centers (-11º<D<-8º) result in more intense convective feedback, associated with reduced SST variability (Fig. 3a). In this case, ENSO frequency is nearly fully entrained in the annual cycle at 1.2±0.06 events per year, thus making El Niño events more predictable. ~~The extreme scenario of strong~~Finally, full equatorward ~~displacement~~ shifts of the convergence zones (D<-12º) ~~of the convection centers~~ indicate~~s~~ a "permanent El Niño" situation~~,~~ and ENSO's frequency is fully entrained into the annual cycle (one event per year)~~in which very intense (>9 mm.day^{-1}) rainfall events occur every year during austral summer (Figure 3a)~~. Thus, indicating these events are not related to intensified anomalous convective feedback but are due to the Convergences Zones being within the equatorial band. ~~In this simulation, continuous high rates of rainfall are associated with a small range (<2ºC) of SST variability (Figure 3a), indicating these events are not related to intensified convective feedback but are, in turn, reflecting the proximity of the climatological position of the convection centers to the equator. In fact, the climatological positions of the ITCZ and SPCZ in the most extreme simulation (3.4ºN and 3.5ºS, respectively) lie within the equatorial band (5ºS-5ºN), in agreement with an amplified warming in the eastern Pacific (dark blue plot in Figure 3a).~~

Another important process in ENSO dynamics is the easterly wind variability in the western Pacific (n~~N~~iño4 region: 160ºE-150ºW). The intensity of the trade winds in the western Pacific has been shown to determine the amplitude of the wind variability in that region (Pontes et al., 2022), which is related to the intensity and frequency of westerly wind bursts, important for ENSO initiation (Chen et al., 2015). In this context, we found that the position of the convection centers also modulates the easterlies' variability through a quadratic relationship (R^2 = 0.51~~2~~; Fig. 3c~~b~~). The two scenarios that show reduced wind variability are consistent with reduced ENSO activity. Poleward movement of the convection centers increases the horizontal scale of the wind flow that reaches the western Pacific, generating wind anomalies in the South Pacific Subtropical High region, indicating that this new regime is more geostrophic, therefore more linearly balanced and deterministic (Fig. 1a-c). On the other hand, strong equatorward shifts of the convection centers require~~s~~ weak horizontal wind intensity within the equatorial band, thus suppressing the development of wind anomalies~~, consistent with weak wind variability~~ (Fig. 3c~~b~~). Despite the consistence between changes in easterly wind variability and the position of the Convergence Zones, changes in wind variability cannot solely explain the nonlinear sensitivity of ENSO across climate states (Fig. 3b). The relationship between changes in easterly wind variability and ENSO is linear and does not distinguish between mean states of reduced (e.g., paleo) and amplified (e.g., future) equatorial warming.

Finally, to investigate the possible modulation of the position of the ~~convection~~ Convergence Zones o~~i~~n the ocean-atmosphere dynamical coupling~~ between the ocean and the atmosphere~~, we analyze the response of the wind-thermocline coefficient (Appendix Text A3) (Jin et al., 2006). This parameter measures the sensitivity of the~~ tilt mode of~~ thermocline slope anomalies to wind stress anomalies, which during El Niño events result in eastward heat advection by downwelling equatorial Kelvin waves (Timmermann et al., 2018). Our results indicate that the displacement of the convection centers also modulates the wind-thermocline coefficient through a quadratic relationship (R^2 = 0.45~~8~~; Fig.~~ure~~ 3d~~e~~). Through affecting the

horizontal wind field, the position of the Convergence Zones underpins the momentum transfer from the atmosphere, influencing oceanic stratification and the thermocline slope in the equatorial Pacific. As s~~S~~trong equatorward shifts of the ~~convection centers~~Convergence Zones drive weak trades and collapsed eastern upwelling, they reduce the effectiveness of wind anomalies in generating swings of the thermocline. ~~In such scenarios~~Furthermore, the propagation of Kelvin waves in a flat~~ter~~ thermocline does not effectively promote oscillations between El Niño and La Ninã ~~states~~anomalies. Poleward shifts of the convection centers increase the climatological thermocline slope, requiring stronger wind to anomalies to promote thermocline oscillation, and thus also reducing the effectiveness of dynamical air-sea coupling.

4. Conclusion

Our findings suggest that meridional shifts of the Convergence Zones modulate key processes for ENSO development, such as~~The results described above suggest a 3-dimensional view of ENSO complexity by linking meridional shifts of the convection centers,~~ equatorial ~~atmospheric~~ convection, trade winds variability ~~ocean stratification,~~ and zonal thermocline oscillations. The interplay of these processes results in a nonlinear ENSO sensitivity to mean states, encompassing three ~~key~~ distinct background conditions deviating from the pre-industrial climate (Fig.~~ure~~ 4): 1)~~.~~ ~~A~~ poleward migration of the convection centers intensifies the easterlies in the equatorial Pacific, weaken~~ing~~ the convective feedback,~~.~~ i~~I~~ncrease~~d~~ momentum transfer to the upper-ocean, reduce~~s~~ ocean stratification and~~,~~ ultimately result~~ing~~ in a weaker dynamical coupling, thus ~~hampering~~ dampening ENSO ~~development (Figure 4). These background conditions~~variability and resembling~~e~~ a La Niña-like mean state (Fig. 4c); 2)~~.~~ m~~M~~oderate equatorward shifts of the convection centers (-8º<D<0º)~~(<9º)~~ reduces the intensity of the equatorial trades and~~,~~ increas~~e~~ing upper-ocean stratification, ~~and~~ consequently amplifying the dynamical air-sea coupling and permitting ~~, which allows the~~ equatorial trades and thermocline slope to be rapidly reversed, thus enhancing ENSO activity and extreme rainfall events (Fig.~~ure~~ 4b);~~.~~ 3) ~~Finally, a~~ strong equatorward shifts of the convection centers create~~s~~ a permanent El

Niño-like mean state in the eastern Pacific. The fact that the convection centers lie at the equator do not allow momentum transfer to the ocean, resulting in a highly stratified ocean and dampened dynamical coupling. Nonetheless, this scenario is associated with intense warming in the eastern Pacific that enhances the climatological thermodynamical coupling, where climatological high SSTs allow continuous intense rainfall ~~every year~~.

The proposed mechanism can reconcile divergences in ENSO responses in proxy-data and modelling studies. First, modelling results from the idealized abrupt4xCO2 simulations indicate inconsistent inter-model ENSO response. We showed that this is related to the sensitivity of ITCZ and SPCZ migrations in each model. This argument can be expanded for meltwater-induced AMOC weakening modelling studies and proxy-data covering Heinrich stadials and the Younger Dryas, which often do not agree on the ENSO response (Glaubke et al., 2024; Liu, 2002; Timmermann et al., 2007). This could be related to the different response of the Pacific Convergence Zones to the intensity and duration of meltwater pulses. Finally, our results provide novel insights into the relationship between ENSO frequency and the annual cycle (Liu, 2002), suggesting that moderate equatorward shift of the Convergence Zones relaxes both mean horizontal and vertical circulations, allowing nonlinear interactions between the annual cycle and ENSO's frequency, thus increasing ENSO's frequency towards the annual cycle. Strong equatorward displacements of the Convergence Zones result in a strong annual cycle associated with an El Niño-like mean state, thus fully entraining ENSO's frequency into the annual cycle and reducing ENSO's interannual variance.~~It is important noting that these results are subject to systematic climate model biases. The main common biases that could affect the processes here analyzed are biases in tropical convection and SST, such as double ITCZs, overly strong cold tongue and predominantly zonally oriented SPCZs (Narsey et al., 2022; Tian & Dong, 2020). Nonetheless, to reduce the influence of such biases, we applied two model selection criteria. Additionally, the artificial calendar effect, due to modified orbital parameters, can reduce the accuracy for LIG and mid- Holocene simulations (Bartlein & Shafer, 2019).~~

~~Climate models~~ Our modelling assessment suggests that the projected increase in ENSO

variability has likely not occurred in the past ~3.3 Ma. While there are significant uncertainties in both paleoclimate simulations and paleo-proxy records, both tend to suggest reduced ENSO variability during the LGM, the LIG and the mid- to late Holocene (Brown et al., 2020; Emile-Geay et al., 2016; Sachs et al., 2009). While these results agree with our understanding of past ITCZ changes (Sachs et al., 2018; Schneider et al., 2014), past dynamics of the SPCZ need to be better understood and constrained to enhance our ability to predict future ENSO behavior.~~(Brown et al., 2020). Nonetheless, state-of-the-art climate models and proxy data initially suggest that the combination of global warming and increased extreme weather events is likely unique to the 21st century. This may reduce the resilience of many species and their adaptation to these unprecedented climate conditions, alerting the global community to a possible great biodiversity loss.~~

Acknowledgments

For their roles in producing, coordinating, and making available CMIP6 and PMIP4 model output, we acknowledge the climate modeling groups (Supplementary Information Table S1), the World Climate Research Programme's Working Group on Coupled Modelling and the Global Organization for Earth System Science Portals. GMP and PLDS acknowledge funding from the São Paulo Research Foundation (grant number 2021/11035-6). This work is supported by the Australian Research Council Special Research Initiative, Australian Centre for Excellence in Antarctic Science (project number SR200100008).

Data and code availability

Simulation from pre-industrial control, future emission scenarios (SSP1-2.6; SSP3-7.0 and SSP5-8.5)~~high emissions scenario (ssp585)~~, mid-Holocene, Last Interglacial, and CESM2, EC-Earth3-LR, NorESM1-F, IPSLCM6A and GISS-E2-1-G simulations of the mid-Pliocene can be obtained directly through the Earth System Grid Federation repository (ESGF; https://esgf-node.llnl.gov/search/cmip6/). Other mid-Pliocene simulations are

available upon request to Alan M. Haywood (a.m.haywood@leeds.ac.uk). Models used in each analysis were selected based on data availability in their respective databases. The last 100 years of each model's simulation are used. All climate periods (paleoclimates and projections) are compared to the pre-industrial climate. Computer codes are available upon request to Gabriel M. Pontes (gabrielpontes@usp.br).

Author contributions

GMP designed the study, conducted the analysis, prepared all figures, and wrote the original manuscript. PLDS and LM contributed with discussions and commented on the manuscript.

Competing interests

At least one of the (co-)authors is a member of the editorial board of Climate of the Past.

References

Brierley, C. M., Zhao, A., Harrison, S. P., Braconnot, P., Williams, C. J. R., Thornalley, D. J. R., Shi, X., Peterschmitt, J. Y., Ohgaito, R., Kaufman, D. S., Kageyama, M., Hargreaves, J. C., Erb, M. P., Emile-Geay, J., D'Agostino, R., Chandan, D., Carré, M., Bartlein, P. J., Zheng, W., Zhang, Z., Zhang, Q., Yang, H., Volodin, E. M., Tomas, R. A., Routson, C., Richard Peltier, W., Otto-Bliesner, B., Morozova, P. A., McKay, N. P., Lohmann, G., Legrande, A. N., Guo, C., Cao, J., Brady, E., Annan, J. D., and Abe-Ouchi, A.: Large-scale features and evaluation of the PMIP4-CMIP6 midHolocene simulations, Climate of the Past, 16, 1847–1872, https://doi.org/10.5194/CP-16-1847-2020, 2020.

Brown, J., Brierley, C., An, S.-I., Guarino, M.-V., Stevenson, S., Williams, C., Zhang, Q., Zhao, A., Braconnot, P., Brady, E., Chandan, D., D'Agostino, R., Guo, C., LeGrande, A., Lohmann, G., Morozova, P., Ohgaito, R., O'ishi, R., Otto-Bliesner, B., Peltier, W. R., Shi, X., Sime, L., Volodin, E., Zhang, Z., and Zheng, W.: Comparison of past and future simulations of ENSO in CMIP5/PMIP3 and CMIP6/PMIP4 models, Climate of The Past Discussions, 1–44, https://doi.org/10.5194/cp-2019-155, 2020.

Burke, K. D., Williams, J. W., Chandler, M. A., Haywood, A. M., Lunt, D. J., and Otto-Bliesner, B. L.: Pliocene and Eocene provide best analogs for near-future climates., Proc Natl Acad Sci U S A, 115, 13288–13293, https://doi.org/10.1073/pnas.1809600115, 2018.

Cai, W., Wang, G., Dewitte, B., Wu, L., Santoso, A., Takahashi, K., Yang, Y., Carréric, A., and McPhaden, M. J.: Increased variability of eastern Pacific El Niño under greenhouse warming, Nature, 564, 201–206, https://doi.org/10.1038/s41586-018-0776-9, 2018.

Cai, W., Santoso, A., Collins, M., Dewitte, B., Karamperidou, C., Kug, J. S., Lengaigne, M., McPhaden, M. J., Stuecker, M. F., Taschetto, A. S., Timmermann, A., Wu, L., Yeh, S. W., Wang, G., Ng, B., Jia, F., Yang, Y., Ying, J., Zheng, X. T., Bayr, T., Brown, J. R., Capotondi, A., Cobb, K. M., Gan, B., Geng, T., Ham, Y. G., Jin, F. F., Jo, H. S., Li, X., Lin, X., McGregor, S., Park, J. H., Stein, K., Yang, K., Zhang, L., and Zhong, W.: Changing El Niño–Southern Oscillation in a warming climate, Nature Reviews Earth & Environment 2021 2:9, 2, 628–644, https://doi.org/10.1038/s43017-021-00199-z, 2021.

Callahan, C. W., Chen, C., Rugenstein, M., Bloch-Johnson, J., Yang, S., and Moyer, E. J.: Robust decrease in El Niño/Southern Oscillation amplitude under long-term warming,

Nature Climate Change 2021 11:9, 11, 752–757, https://doi.org/10.1038/s41558-021-01099-2, 2021.

Chen, D., Lian, T., Fu, C., Cane, M. A., Tang, Y., Murtugudde, R., Song, X., Wu, Q., and Zhou, L.: Strong influence of westerly wind bursts on El Niño diversity, https://doi.org/10.1038/ngeo2399, 30 May 2015.

Chen, L., Zheng, W., and Braconnot, P.: Towards understanding the suppressed ENSO activity during mid-Holocene in PMIP2 and PMIP3 simulations, Clim Dyn, 53, 1095–1110, https://doi.org/10.1007/s00382-019-04637-z, 2019.

Dommenget, D., Bayr, T., and Frauen, C.: Analysis of the non-linearity in the pattern and time evolution of El Niño southern oscillation, Climate Dynamics 2012 40:11, 40, 2825–2847, https://doi.org/10.1007/S00382-012-1475-0, 2012.

Emile-Geay, J., Cobb, K. M., Carre, M., Braconnot, P., Leloup, J., Zhou, Y., Harrison, S. P., Corrège, T., McGregor, H. V., Collins, M., Driscoll, R., Elliot, M., Schneider, B., and Tudhope, A.: Links between tropical Pacific seasonal, interannual and orbital variability during the Holocene, https://doi.org/10.1038/ngeo2608, 1 February 2016.

Ford, H. L., Ravelo, A. C., and Polissar, P. J.: Reduced El Niño-Southern Oscillation during the last glacial maximum, Science (1979), 347, 255–258, https://doi.org/10.1126/science.1258437, 2015.

Glaubke, R. H., Schmidt, M. W., Hertzberg, J. E., Ward, L. G., Marcantonio, F., Schimmenti, D., and Thirumalai, K.: An Inconsistent ENSO Response to Northern Hemisphere Stadials Over the Last Deglaciation, Geophys Res Lett, 51, e2023GL107634, https://doi.org/10.1029/2023GL107634, 2024.

Haywood, A. M., Tindall, J. C., Dowsett, H. J., Dolan, A. M., Foley, K. M., Hunter, S. J., Hill, D. J., Chan, W.-L., Abe-Ouchi, A., Stepanek, C., Lohmann, G., Chandan, D., Peltier, W. R., Tan, N., Contoux, C., Ramstein, G., Li, X., Zhang, Z., Guo, C., Nisancioglu, K. H., Zhang, Q., Li, Q., Kamae, Y., Chandler, M. A., Sohl, L. E., Otto-Bliesner, B. L., Feng, R., Brady, E. C., von der Heydt, A. S., Baatsen, M. L. J., and Lunt, D. J.: The Pliocene Model Intercomparison Project Phase 2: large-scale climate features and climate sensitivity, Climate of the Past, 16, 2095–2123, https://doi.org/10.5194/cp-16-2095-2020, 2020.

Jin, F. F., Kim, S. T., and Bejarano, L.: A coupled-stability index for ENSO, Geophys Res Lett, 33, L23708, https://doi.org/10.1029/2006GL027221, 2006.

Johnson, N. C. and Xie, S. P.: Changes in the sea surface temperature threshold for tropical convection, Nat Geosci, 3, 842–845, https://doi.org/10.1038/ngeo1008, 2010.

Kageyama, M., Harrison, S. P., Kapsch, M. L., Lofverstrom, M., Lora, J. M., Mikolajewicz, U., Sherriff-Tadano, S., Vadsaria, T., Abe-Ouchi, A., Bouttes, N., Chandan, D., Gregoire, L. J., Ivanovic, R. F., Izumi, K., Legrande, A. N., Lhardy, F., Lohmann, G., Morozova, P. A., Ohgaito, R., Paul, A., Richard Peltier, W., Poulsen, C. J., Quiquet, A., Roche, D. M., Shi, X., Tierney, J. E., Valdes, P. J., Volodin, E., and Zhu, J.: The PMIP4 Last Glacial Maximum experiments: Preliminary results and comparison with the PMIP3 simulations, Climate of the Past, 17, 1065–1089, https://doi.org/10.5194/CP-17-1065-2021, 2021.

Liu, Z.: A Simple Model Study of ENSO Suppression by External Periodic Forcing, J Clim, 15, 1088–1098, https://doi.org/10.1175/1520-0442(2002)015, 2002.

Lunt, D. J., Haywood, A. M., Schmidt, G. A., Salzmann, U., Valdes, P. J., Dowsett, H. J., and Loptson, C. A.: On the causes of mid-Pliocene warmth and polar amplification, Earth Planet Sci Lett, 321–322, 128–138, https://doi.org/10.1016/j.epsl.2011.12.042, 2012.

Marcott, S. A., Bauska, T. K., Buizert, C., Steig, E. J., Rosen, J. L., Cuffey, K. M., Fudge, T.

J., Severinghaus, J. P., Ahn, J., Kalk, M. L., McConnell, J. R., Sowers, T., Taylor, K. C., White, J. W. C., and Brook, E. J.: Centennial-scale changes in the global carbon cycle during the last deglaciation, Nature 2014 514:7524, 514, 616–619, https://doi.org/10.1038/nature13799, 2014.

O'neill, B. C., Tebaldi, C., Van Vuuren, D. P., Eyring, V., Friedlingstein, P., Hurtt, G., Knutti, R., Kriegler, E., Lamarque, J.-F., Lowe, J., Meehl, G. A., Moss, R., Riahi, K., and Sanderson, B. M.: The Scenario Model Intercomparison Project (ScenarioMIP) for CMIP6, Geosci. Model Dev, 9, 3461–3482, https://doi.org/10.5194/gmd-9-3461-2016, 2016.

Otto-Bliesner, B. L., Brady, E. C., Zhao, A., Brierley, C. M., Axford, Y., Capron, E., Govin, A., Hoffman, J. S., Isaacs, E., Kageyama, M., Scussolini, P., Tzedakis, P. C., Williams, C. J. R., Wolff, E., Abe-Ouchi, A., Braconnot, P., Ramos Buarque, S., Cao, J., de Vernal, A., Guarino, M. V., Guo, C., LeGrande, A. N., Lohmann, G., Meissner, K. J., Menviel, L., Morozova, P. A., Nisancioglu, K. H., O'ishi, R., Salas y Mélia, D., Shi, X., Sicard, M., Sime, L., Stepanek, C., Tomas, R., Volodin, E., Yeung, N. K. H., Zhang, Q., Zhang, Z., and Zheng, W.: Large-scale features of Last Interglacial climate: results from evaluating the <i>lig127k</i> simulations for the Coupled Model Intercomparison Project (CMIP6)–Paleoclimate Modeling Intercomparison Project (PMIP4), Climate of the Past, 17, 63–94, https://doi.org/10.5194/cp-17-63-2021, 2021.

PAGES working Group: Interglacials of the last 800,000 years, Reviews of Geophysics, 54, 162–219, https://doi.org/10.1002/2015RG000482, 2016.

Pausata, F. S. R., Zhang, Q., Muschitiello, F., Lu, Z., Chafik, L., Niedermeyer, E. M., Stager, J. C., Cobb, K. M., and Liu, Z.: Greening of the Sahara suppressed ENSO activity during the mid-Holocene, Nat Commun, 8, https://doi.org/10.1038/ncomms16020, 2017.

Peng, Q., Xie, S. P., and Deser, C.: Collapsed upwelling projected to weaken ENSO under sustained warming beyond the twenty-first century, Nature Climate Change 2024 14:8, 14, 815–822, https://doi.org/10.1038/s41558-024-02061-8, 2024.

Pontes, G., Dias, P. S., and Menviel, L.: Paleoclimate constrains future El Niño/Southern Oscillation increase, https://doi.org/10.21203/RS.3.RS-2062789/V1, 2022a.

Pontes, G. M., Wainer, I., Taschetto, A. S., Sen Gupta, A., Abe-Ouchi, A., Brady, E. C., Chan, W.-L., Chandan, D., Contoux, C., Feng, R., Hunter, S. J., Kame, Y., Lohmann, G., Otto-Bliesner, B. L., Peltier, W. R., Stepanek, C., Tindall, J., Tan, N., Zhang, Q., and Zhang, Z.: Drier tropical and subtropical Southern Hemisphere in the mid-Pliocene Warm Period, Sci Rep, 10, 13458, https://doi.org/10.1038/s41598-020-68884-5, 2020.

Pontes, G. M., Taschetto, A. S., Sen Gupta, A., Santoso, A., Wainer, I., Haywood, A. M., Chan, W.-L., Abe-Ouchi, A., Stepanek, C., Lohmann, G., Hunter, S. J., Tindall, J. C., Chandler, M. A., Sohl, L. E., Peltier, W. R., Chandan, D., Kamae, Y., Nisancioglu, K. H., Zhang, Z., Contoux, C., Tan, N., Zhang, Q., Otto-Bliesner, B. L., Brady, E. C., Feng, R., von der Heydt, A. S., Baatsen, M. L. J., and Oldeman, A. M.: Mid-Pliocene El Niño/Southern Oscillation suppressed by Pacific intertropical convergence zone shift, Nature Geoscience 2022, 1–9, https://doi.org/10.1038/s41561-022-00999-y, 2022b.

Ropelewski, C. F. and Halpert, M. S.: Global and Regional Scale Precipitation Patterns Associated with the El Niño/Southern Oscillation, Mon Weather Rev, 115, 1606–1626, https://doi.org/https://doi.org/10.1175/1520-0493(1987)115<1606:GARSPP>2.0.CO;2, 1987.

Sachs, J. P., Sachse, D., Smittenberg, R. H., Zhang, Z., Battisti, D. S., and Golubic, S.: Southward movement of the Pacific intertropical convergence zone AD 1400–1850, Nat Geosci, 2, 519–525, https://doi.org/10.1038/ngeo554, 2009.

Sachs, J. P., Blois, J. L., McGee, T., Wolhowe, M., Haberle, S., Clark, G., and Atahan, P.: Southward Shift of the Pacific ITCZ During the Holocene, Paleoceanogr Paleoclimatol, 33, 1383–1395, https://doi.org/10.1029/2018PA003469, 2018.

Schneider, T., Bischoff, T., and Haug, G. H.: Migrations and dynamics of the intertropical convergence zone., Nature, 513, 45–53, https://doi.org/10.1038/nature13636, 2014.

Takahashi, K., Montecinos, A., Goubanova, K., and Dewitte, B.: ENSO regimes: Reinterpreting the canonical and Modoki El Niño, Geophys Res Lett, 38, https://doi.org/10.1029/2011GL047364, 2011.

Thirumalai, K., DiNezio, P. N., Partin, J. W., Liu, D., Costa, K., and Jacobel, A.: Future increase in extreme El Niño supported by past glacial changes, Nature 2024 634:8033, 634, 374–380, https://doi.org/10.1038/s41586-024-07984-y, 2024.

Timmermann, A., Okumura, Y., An, S. I., Clement, A., Dong, B., Guilyardi, E., Hu, A., Jungclaus, J. H., Renold, M., Stocker, T. F., Stouffer, R. J., Sutton, R., Xie, S. P., and Yin, J.: The Influence of a Weakening of the Atlantic Meridional Overturning Circulation on ENSO, J Clim, 20, 4899–4919, https://doi.org/10.1175/JCLI4283.1, 2007.

Timmermann, A., An, S. Il, Kug, J. S., Jin, F. F., Cai, W., Capotondi, A., Cobb, K., Lengaigne, M., McPhaden, M. J., Stuecker, M. F., Stein, K., Wittenberg, A. T., Yun, K. S., Bayr, T., Chen, H. C., Chikamoto, Y., Dewitte, B., Dommenget, D., Grothe, P., Guilyardi, E., Ham, Y. G., Hayashi, M., Ineson, S., Kang, D., Kim, S., Kim, W. M., Lee, J. Y., Li, T., Luo, J. J., McGregor, S., Planton, Y., Power, S., Rashid, H., Ren, H. L., Santoso, A., Takahashi, K., Todd, A., Wang, G., Wang, G., Xie, R., Yang, W. H., Yeh, S. W., Yoon, J., Zeller, E., and Zhang, X.: El Niño–Southern Oscillation complexity, https://doi.org/10.1038/s41586-018-0252-6, 26 July 2018.

Vimont, D. J., Battisti, D. S., and Hirst, A. C.: Footprinting: A seasonal connection between the tropics and mid-latitudes, Geophys Res Lett, 28, 3923–3926, https://doi.org/10.1029/2001GL013435, 2001.

Watanabe, T., Suzuki, A., Minobe, S., Kawashima, T., Kameo, K., Minoshima, K., Aguilar, Y. M., Wani, R., Kawahata, H., Sowa, K., Nagai, T., and Kase, T.: Permanent El Niño during the Pliocene warm period not supported by coral evidence, Nature, 471, 209–211, https://doi.org/10.1038/nature09777, 2011.

White, S. M. and Ravelo, A. C.: Dampened El Niño in the Early Pliocene Warm Period, Geophys Res Lett, 47, e2019GL085504, https://doi.org/10.1029/2019GL085504, 2020.

Zheng, Y., Rugenstein, M., Pieper, P., Beobide-Arsuaga, G., and Baehr, J.: El Niño–Southern Oscillation (ENSO) predictability in equilibrated warmer climates, Earth System Dynamics, 13, 1611–1623, https://doi.org/10.5194/ESD-13-1611-2022, 2022.

~~Bartlein, P. J., & Shafer, S. L. (2019). Paleo calendar-effect adjustments in time-slice and transient climate-model simulations (PaleoCalAdjust v1.0): impact and strategies for data analysis. *Geoscientific Model Development*, *12*(9), 3889–3913. https://doi.org/10.5194/GMD-12-3889-2019~~

~~Berger, B., Crucifix, M., Hodell, D. A., Mangili, C., McManus, J. F., Otto-Bliesner, B., Pol, K., Raynaud, D., Skinner, L. C., Tzedakis, P. C., Wolff, E. W., Yin, Q. Z., Abe-Ouchi, A., Barbante, C., Brovkin, V., Cacho, I., Capron, E., Ferretti, P., Ganopolski, A., … Vazquez Riveiros, N. (2016). Interglacials of the last 800,000 years. *Reviews of Geophysics*, *54*(1), 162–~~

219. https://doi.org/10.1002/2015RG000482

Brierley, C. M., Zhao, A., Harrison, S. P., Braconnot, P., Williams, C. J. R., Thornalley, D. J. R., Shi, X., Peterschmitt, J. Y., Ohgaito, R., Kaufman, D. S., Kageyama, M., Hargreaves, J. C., Erb, M. P., Emile-Geay, J., D'Agostino, R., Chandan, D., Carré, M., Bartlein, P. J., Zheng, W., … Abe-Ouchi, A. (2020). Large-scale features and evaluation of the PMIP4-CMIP6 midHolocene simulations. *Climate of the Past*, *16*(5), 1847–1872. https://doi.org/10.5194/CP-16-1847-2020

Brown, J., Brierley, C., An, S.-I., Guarino, M.-V., Stevenson, S., Williams, C., Zhang, Q., Zhao, A., Braconnot, P., Brady, E., Chandan, D., D'Agostino, R., Guo, C., LeGrande, A., Lohmann, G., Morozova, P., Ohgaito, R., O'ishi, R., Otto-Bliesner, B., … Zheng, W. (2020). Comparison of past and future simulations of ENSO in CMIP5/PMIP3 and CMIP6/PMIP4 models. *Climate of The Past Discussions*, 1–44. https://doi.org/10.5194/cp-2019-155

Brown, J. R., Lengaigne, M., Lintner, B. R., Widlansky, M. J., van der Wiel, K., Dutheil, C., Linsley, B. K., Matthews, A. J., & Renwick, J. (2020). South Pacific Convergence Zone dynamics, variability and impacts in a changing climate. *Nature Reviews Earth & Environment*, 1–14. https://doi.org/10.1038/s43017-020-0078-2

Cai, W., Wang, G., Dewitte, B., Wu, L., Santoso, A., Takahashi, K., Yang, Y., Carréric, A., & McPhaden, M. J. (2018). Increased variability of eastern Pacific El Niño under greenhouse warming. *Nature*, *564*(7735), 201–206. https://doi.org/10.1038/s41586-018-0776-9

Chen, D., Lian, T., Fu, C., Cane, M. A., Tang, Y., Murtugudde, R., Song, X., Wu, Q., & Zhou, L. (2015). Strong influence of westerly wind bursts on Elo diversity. In *Nature Geoscience* (Vol. 8, Issue 5, pp. 339–345). Nature Publishing Group. https://doi.org/10.1038/ngeo2399

Chiang, J. C. H., Fang, Y., & Chang, P. (2008). Interhemispheric thermal gradient and tropical Pacific climate. *Geophysical Research Letters*, *35*(14). https://doi.org/10.1029/2008GL034166

De Schepper, S., Gibbard, P. L., Salzmann, U., & Ehlers, J. (2014). A global synthesis of the marine and terrestrial evidence for glaciation during the Pliocene Epoch. *Earth-Science Reviews*, *135*, 83–102. https://doi.org/10.1016/j.earscirev.2014.04.003

Dommenget, D., Bayr, T., & Frauen, C. (2012). Analysis of the non-linearity in the pattern and time evolution of El Niño southern oscillation. *Climate Dynamics 2012 40:11*, *40*(11), 2825–2847. https://doi.org/10.1007/S00382-012-1475-0

Emile-Geay, J., Cobb, K. M., Carre, M., Braconnot, P., Leloup, J., Zhou, Y., Harrison, S. P., Corrège, T., McGregor, H. V., Collins, M., Driscoll, R., Elliot, M., Schneider, B., & Tudhope, A. (2016). Links between tropical Pacific seasonal, interannual and orbital variability during the Holocene. In *Nature Geoscience* (Vol. 9, Issue 2, pp. 168–173). Nature Publishing Group. https://doi.org/10.1038/ngeo2608

Fedorov, A. V., Burls, N. J., Lawrence, K. T., & Peterson, L. C. (2015). Tightly linked zonal and meridional sea surface temperature gradients over the past five million years. *Nature Geoscience*, *8*(12), 975–980. https://doi.org/10.1038/ngeo2577 during the last glacial maximum. *Science*, *347*(6219), 255–258. https://doi.org/10.1126/science.1258437

Haywood, A. M., Tindall, J. C., Dowsett, H. J., Dolan, A. M., Foley, K. M., Hunter, S. J., Hill, D. J., Chan, W.-L., Abe-Ouchi, A., Stepanek, C., Lohmann, G., Chandan, D., Peltier, W. R., Tan, N., Contoux, C., Ramstein, G., Li, X., Zhang, Z., Guo, C., … Lunt, D. J. (2020). The Pliocene Model Intercomparison Project Phase 2: large-scale climate features and climate sensitivity. *Climate of the Past*, *16*(6), 2095–2123. https://doi.org/10.5194/cp-16-2095-2020

Hu, S., & Fedorov, A. V. (2018). Cross-equatorial winds control El Niño diversity and change. In

Nature Climate Change (Vol. 8, Issue 9, pp. 798–802). Nature Publishing Group. https://doi.org/10.1038/s41558-018-0248-0

Jin, F. F., Kim, S. T., & Bejarano, L. (2006). A coupled stability index for ENSO. *Geophysical Research Letters*, *33*(23), L23708. https://doi.org/10.1029/2006GL027221

Johnson, N. C., & Xie, S. P. (2010). Changes in the sea surface temperature threshold for tropical convection. *Nature Geoscience*, *3*(12), 842–845. https://doi.org/10.1038/ngeo1008

Liu, C., An, S. Il, Jin, F. F., Shin, J., Kug, J. S., Zhang, W., Stuecker, M. F., Yuan, X., Xue, A., Geng, X., & Kim, S. K. (2023). Hysteresis of the El Niño–Southern Oscillation to CO2 forcing. *Science Advances*, *9*(31). https://doi.org/10.1126/SCIADV.ADH8442/SUPPL_FILE/SCIADV.ADH8442_SM.PDF

Liu, Z. (2002). A simple model study of ENSO suppression by external periodic forcing. *Journal of Climate*, *15*(9), 1088–1098. https://doi.org/10.1175/1520-0442(2002)015<1088:ASMSOE>2.0.CO;2

Lunt, D. J., Haywood, A. M., Schmidt, G. A., Salzmann, U., Valdes, P. J., Dowsett, H. J., & Loptson, C. A. (2012). On the causes of mid-Pliocene warmth and polar amplification. *Earth and Planetary Science Letters*, *321–322*, 128–138. https://doi.org/10.1016/j.epsl.2011.12.042

Mamalakis, A., Randerson, J. T., Yu, J.-Y., Pritchard, M. S., Magnusdottir, G., Smyth, P., Levine, P. A., Yu, S., & Foufoula-Georgiou, E. (2021). Zonally contrasting shifts of the tropical rain belt in response to climate change. *Nature Climate Change*, 1–9. https://doi.org/10.1038/s41558-020-00963-x

Narsey, S., Brown, J. R., Delage, F., Boschat, G., Grose, M., Colman, R., & Power, S. (2022). Storylines of South Pacific Convergence Zone changes in a warmer world. *Journal of Climate*, *1*(aop), 1–59. https://doi.org/10.1175/JCLI-D-21-0433.1

O'neill, B. C., Tebaldi, C., Van Vuuren, D. P., Eyring, V., Friedlingstein, P., Hurtt, G., Knutti, R., Kriegler, E., Lamarque, J.-F., Lowe, J., Meehl, G. A., Moss, R., Riahi, K., & Sanderson, B. M. (2016). The Scenario Model Intercomparison Project (ScenarioMIP) for CMIP6. *Geosci. Model Dev*, *9*, 3461–3482. https://doi.org/10.5194/gmd-9-3461-2016

Otto-Bliesner, B. L., Brady, E. C., Zhao, A., Brierley, C. M., Axford, Y., Capron, E., Govin, A., Hoffman, J. S., Isaacs, E., Kageyama, M., Scussolini, P., Tzedakis, P. C., Williams, C. J. R., Wolff, E., Abe-Ouchi, A., Braconnot, P., Ramos Buarque, S., Cao, J., de Vernal, A., … Zheng, W. (2021). Large-scale features of Last Interglacial climate: results from evaluating the <i>lig127k</i> simulations for the Coupled Model Intercomparison Project (CMIP6)–Paleoclimate Modeling Intercomparison Project (PMIP4). *Climate of the Past*, *17*(1), 63–94. https://doi.org/10.5194/cp-17-63-2021

Pausata, F. S. R., Zhang, Q., Muschitiello, F., Lu, Z., Chafik, L., Niedermeyer, E. M., Stager, J. C., Cobb, K. M., & Liu, Z. (2017). Greening of the Sahara suppressed ENSO activity during the mid-Holocene. *Nature Communications*, *8*. https://doi.org/10.1038/ncomms16020

Pontes, G. M., Taschetto, A. S., Sen Gupta, A., Santoso, A., Wainer, I., Haywood, A. M., Chan, W.-L., Abe-Ouchi, A., Stepanek, C., Lohmann, G., Hunter, S. J., Tindall, J. C., Chandler, M.

A., Sohl, L. E., Peltier, W. R., Chandan, D., Kamae, Y., Nisancioglu, K. H., Zhang, Z., … Oldeman, A. M. (2022). Mid-Pliocene El Niño/Southern Oscillation suppressed by Pacific intertropical convergence zone shift. *Nature Geoscience 2022*, 1–9. https://doi.org/10.1038/s41561-022-00999-y

Pontes, G. M., Wainer, I., Taschetto, A. S., Sen Gupta, A., Abe-Ouchi, A., Brady, E. C., Chan, W. L., Chandan, D., Contoux, C., Feng, R., Hunter, S. J., Kame, Y., Lohmann, G., Otto-

Bliesner, B. L., Peltier, W. R., Stepanek, C., Tindall, J., Tan, N., Zhang, Q., & Zhang, Z. (2020). Drier tropical and subtropical Southern Hemisphere in the mid-Pliocene Warm Period. *Scientific Reports*, *10*(1), 13458. https://doi.org/10.1038/s41598-020-68884-5

Ropelewski, C. F., & Halpert, M. S. (1987). Global and Regional Scale Precipitation Patterns Associated with the El Niño/Southern Oscillation. *Monthly Weather Review*, *115*(8), 1606–1626. https://doi.org/https://doi.org/10.1175/1520-0493(1987)115<1606:GARSPP>2.0.CO;2

Sachs, J. P., Blois, J. L., McGee, T., Wolhowe, M., Haberle, S., Clark, G., & Atahan, P. (2018). Southward Shift of the Pacific ITCZ During the Holocene. *Paleoceanography and Paleoclimatology*, *33*(12), 1383–1395. https://doi.org/10.1029/2018PA003469

Sachs, J. P., Sachse, D., Smittenberg, R. H., Zhang, Z., Battisti, D. S., & Golubic, S. (2009). Southward movement of the Pacific intertropical convergence zone AD 1400–1850. *Nature Geoscience*, *2*(7), 519–525. https://doi.org/10.1038/ngeo554

Sadekov, A. Y., Ganeshram, R., Pichevin, L., Berdin, R., McClymont, E., Elderfield, H., & Tudhope, A. W. (2013). Palaeoclimate reconstructions reveal a strong link between El Niño-Southern Oscillation and Tropical Pacific mean state. *Nature Communications 2013 4:1*, *4*(1), 1–8. https://doi.org/10.1038/ncomms3692

Santoso, A., McGregor, S., Jin, F. F., Cai, W., England, M. H., An, S. Il, McPhaden, M. J., & Guilyardi, E. (2013). Late-twentieth-century emergence of the El Niño propagation asymmetry and future projections. *Nature*, *504*(7478), 126–130. https://doi.org/10.1038/nature12683

Schneider, T., Bischoff, T., & Haug, G. H. (2014). Migrations and dynamics of the intertropical convergence zone. *Nature*, *513*(7516), 45–53. https://doi.org/10.1038/nature13636

Shin, N. Y., Kug, J. S., Stuecker, M. F., Jin, F. F., Timmermann, A., & Kim, G. Il. (2022). More frequent central Pacific El Niño and stronger eastern pacific El Niño in a warmer climate. *Npj Climate and Atmospheric Science 2022 5:1*, *5*(1), 1–8. https://doi.org/10.1038/s41612-022-00324-9

Takahashi, K., Montecinos, A., Goubanova, K., & Dewitte, B. (2011). ENSO regimes: Reinterpreting the canonical and Modoki El Niño. *Geophysical Research Letters*, *38*(10). https://doi.org/10.1029/2011GL047364

Taschetto, A. S., Sen Gupta, A., Jourdain, N. C., Santoso, A., Ummenhofer, C. C., & England, M. H. (2014). Cold Tongue and Warm Pool ENSO Events in CMIP5: Mean State and Future Projections. *Journal of Climate*, *27*, 2861–2885. https://doi.org/10.1175/JCLI-D-13-00437.1

Tian, B., & Dong, X. (2020). The Double-ITCZ Bias in CMIP3, CMIP5, and CMIP6 Models Based on Annual Mean Precipitation. *Geophysical Research Letters*, *47*(8), e2020GL087232. https://doi.org/10.1029/2020GL087232

Timmermann, A., An, S. Il, Kug, J. S., Jin, F. F., Cai, W., Capotondi, A., Cobb, K., Lengaigne, M., McPhaden, M. J., Stuecker, M. F., Stein, K., Wittenberg, A. T., Yun, K. S., Bayr, T., Chen, H. C., Chikamoto, Y., Dewitte, B., Dommenget, D., Grothe, P., … Zhang, X. (2018). El Niño–Southern Oscillation complexity. In *Nature* (Vol. 559, Issue 7715, pp. 535–545). Nature Publishing Group. https://doi.org/10.1038/s41586-018-0252-6

Tudhope, A. W., Chilcott, C. P., McCulloch, M. T., Cook, E. R., Chappell, J., Ellam, R. M., Lea, D. W., Lough, J. M., & Shimmield, G. B. (2001). Variability in the El Niño Southern Oscillation through a glacial interglacial cycle. *Science*, *291*(5508), 1511–1517. https://doi.org/10.1126/SCIENCE.1057969/SUPPL_FILE/1057969S1_THUMB.GIF

van der Lubbe, H. J. L., Hall, I. R., Barker, S., Hemming, S. R., Baars, T. F., Starr, A., Just, J., Backeberg, B. C., & Joordens, J. C. A. (2021). Indo-Pacific Walker circulation drove

Pleistocene African aridification. *Nature 2021 598:7882*, *598*(7882), 618–623. https://doi.org/10.1038/s41586-021-03896-3

Watanabe, T., Suzuki, A., Minobe, S., Kawashima, T., Kameo, K., Minoshima, K., Aguilar, Y. M., Wani, R., Kawahata, H., Sowa, K., Nagai, T., & Kase, T. (2011). Permanent El Niño during the Pliocene warm period not supported by coral evidence. *Nature*, *471*(7337), 209–211. https://doi.org/10.1038/nature09777

White, S. M., & Ravelo, A. C. (2020). Dampened El Niño in the Early Pliocene Warm Period.

Figures

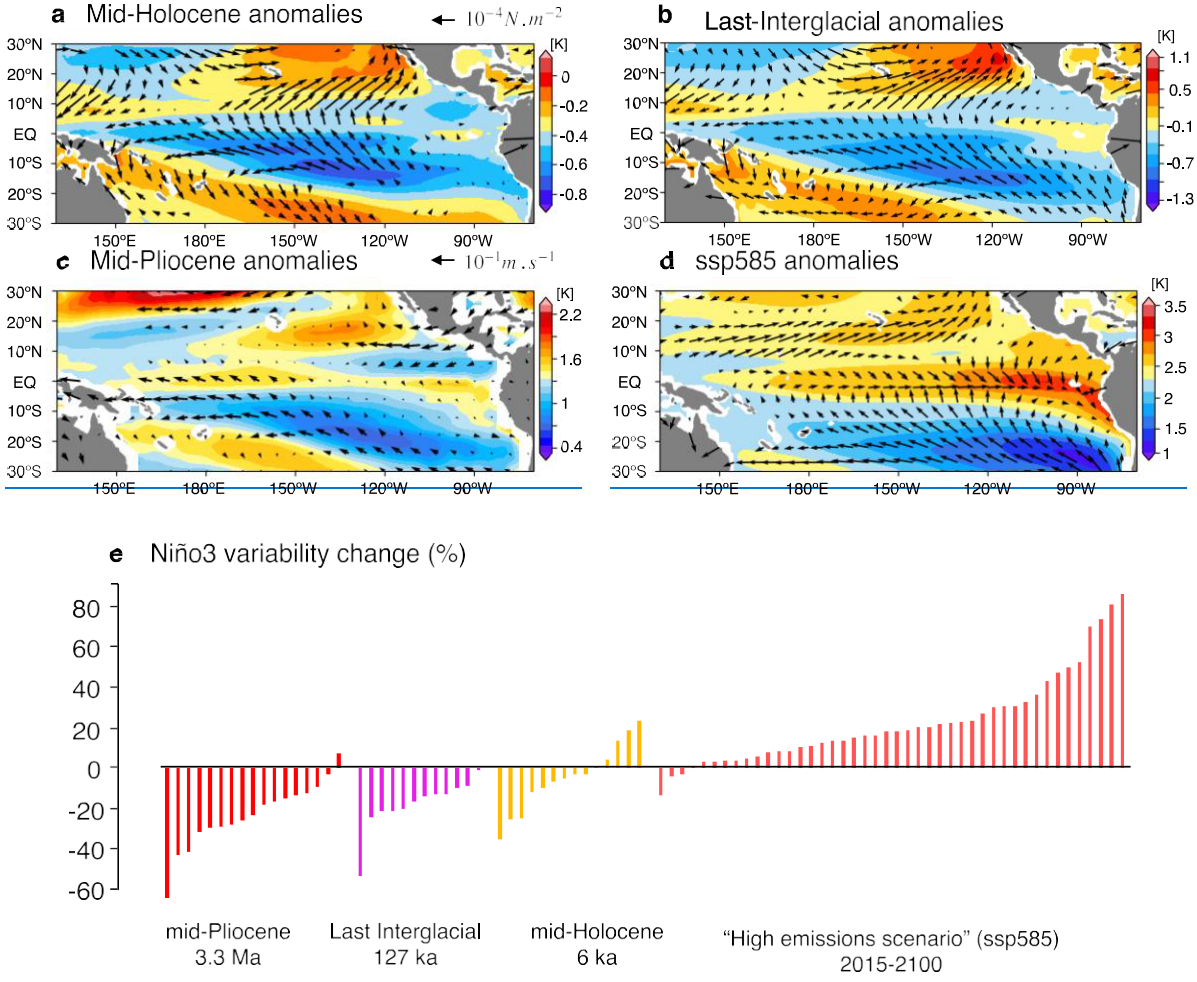
a Mid-Holocene anomalies
$10^{-4} N.m^{-2}$
b Last-Interglacial anomalies
c Mid-Pliocene anomalies
$10^{-1} m.s^{-1}$
d ssp585 anomalies
[K]
30°N
20°N
10°N
EQ
10°S
20°S
30°S
150°E
180°E
150°W
120°W
90°W
0
-0.2
-0.4
-0.6
-0.8
1.1
0.5
-0.1
-0.7
-1.3
2.2
1.6
1
0.4
3.5
3
2.5
2
1.5
1

e Niño3 variability change (%)
80
60
40
20
0
-20
-40
-60
mid-Pliocene
3.3 Ma
Last Interglacial
127 ka
mid-Holocene
6 ka
"High emissions scenario" (ssp585)
2015-2100

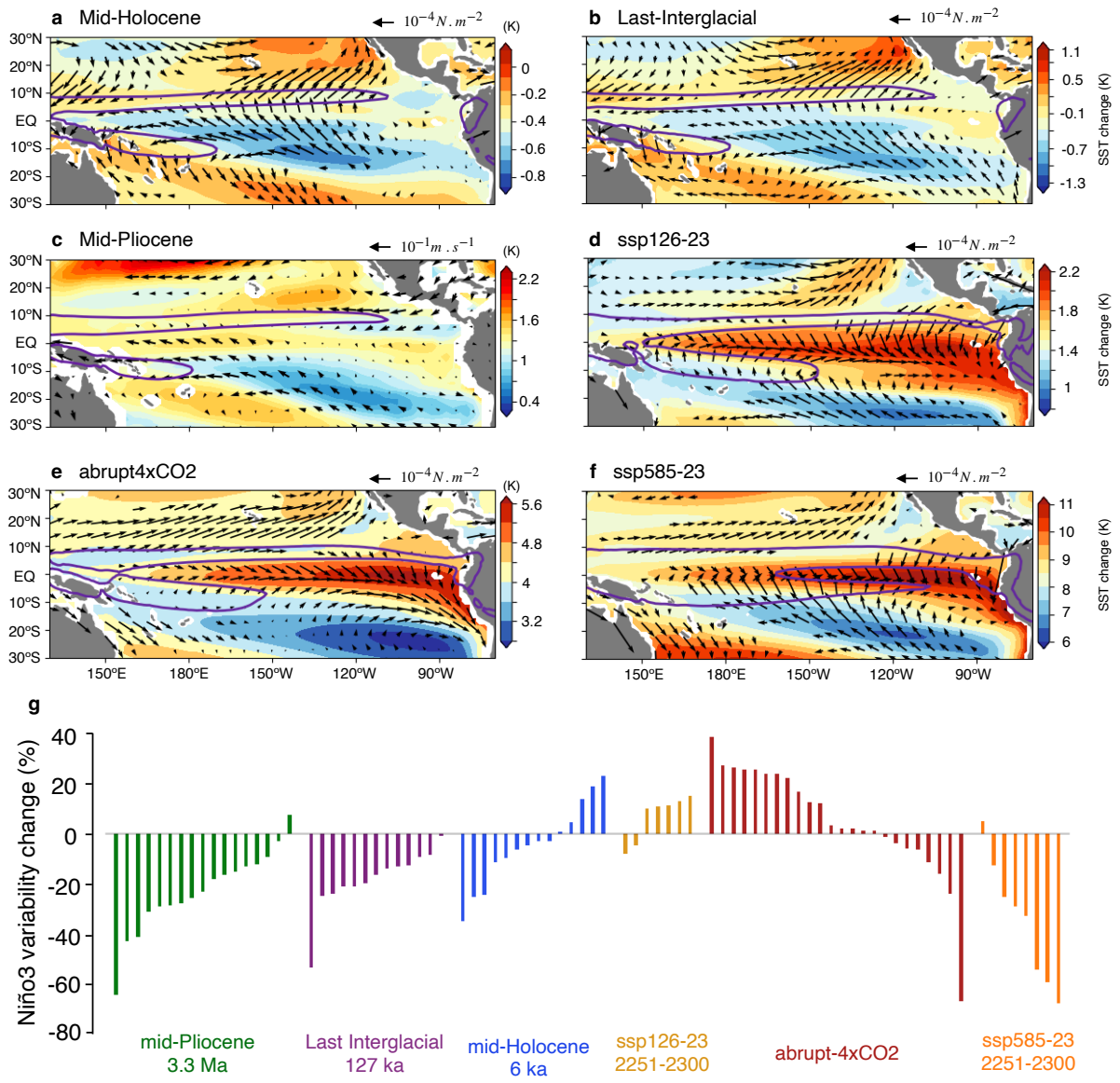

Fig. 1. Paleoclimate anomalies and ENSO variability change. a-d Multi-model annual mean change in SST and wind field for the mid-Holocene (**a**), Last-interglacial (**b**), mid-Pliocene (**c**), ssp126-23 (**d**), abrupt-4xCO2 (**e**), and ssp585-23 (**f**). ~~and high emissions scenario (ssp585; **d**).~~ The SST colorbar varies for each panel~~. The colorbar is set~~ to highlight ~~indicate~~ regions ~~in which~~where SST changes are greater (warm colors) and lower (cold colors) than the mean tropical Pacific warming in each set of simulations, making changes in SST gradients easily identified. Arrows represent wind stress changes in all panels ~~**a, b and d and**~~but panel **c**, where they represent ~~changes in surface winds,~~ due to data availability~~due to data availability, surface (10-meter) winds in panel **c**~~. Arrows are plotted where there is a significant change in either zonal or meridional component ~~. That is, at least a~~(~~-~~70% model agreement in the sign of the change). Purple lines indicate the multi-model mean 8 mm day^{-1} climatological rainfall contours for each time slice as an estimate of the ITCZ and SPCZ positions. **g~~e~~** Change in niño3 standard deviation for each simulation used in this study. The pre-industrial control simulation is used as reference when quantifying changes. ~~The value~~Values for each simulation can be found in Supplementary Information Tables S1~~ and S2~~. Analyses shown in this figure include results from all models, with no selection criteria being applied. Maps in this figure were plotted using the cartopy Python library.

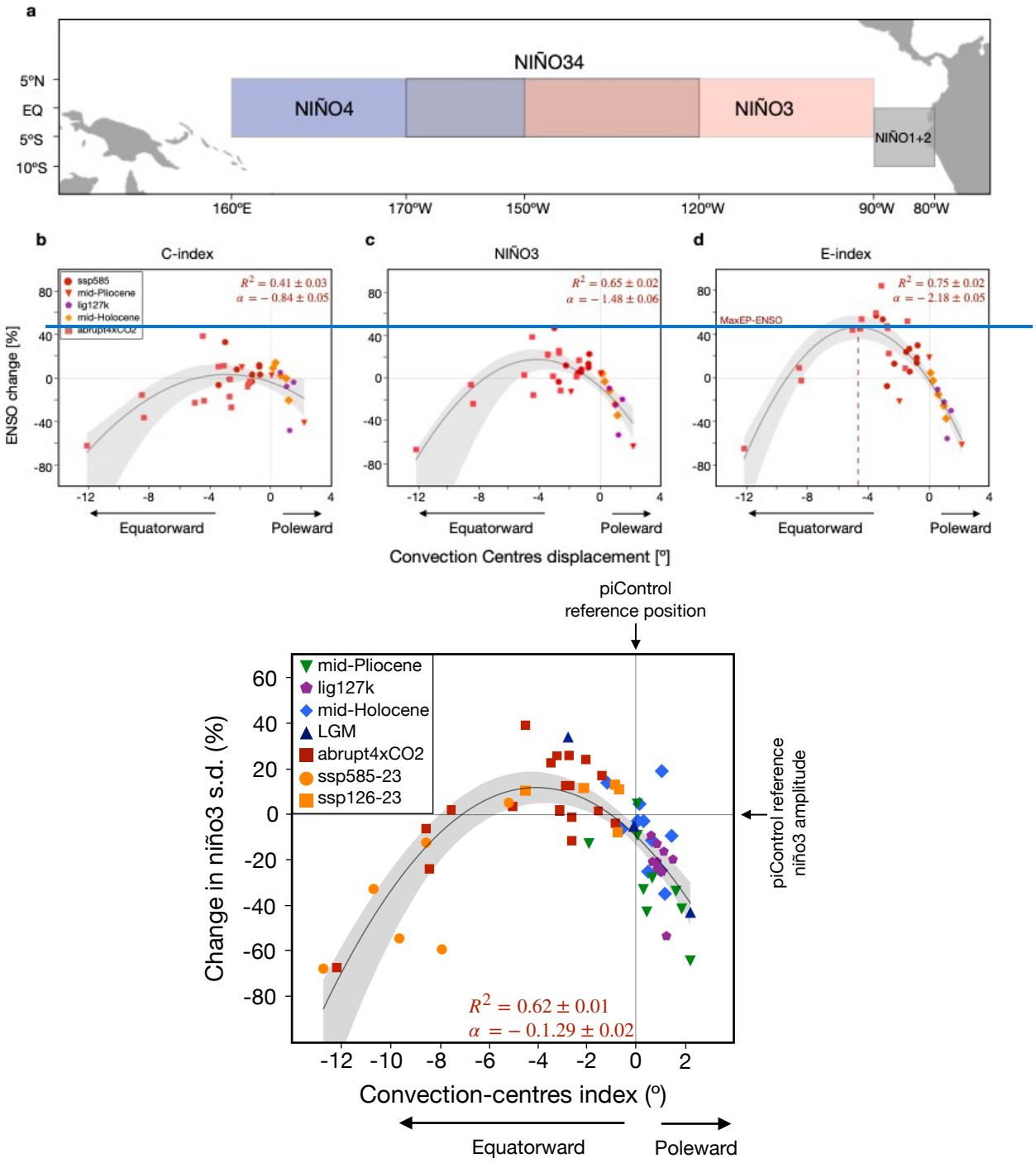

Fig. 2. ENSO-Convection Centers relationship. **Nonlinear ENSO sensitivity across climate states.** Relationship between the convection-centres index and the change in niño3 amplitude, measured by its standard deviation (s.d.). ~~**a** Location of key ENSO regions. **b-d** Dispersion diagram between the overall displacement in the meridional position of the ITCZ and SPCZ and ENSO indices. **b** C-index. **c** E-index. **d** Niño3 index. The s~~Solid black line indicates the quadratic fit based on the least squares method. Banding indicates 95% confidence interval based on a 1,000-sample bootstrap. The mean displacement of the convection centers boreal spring-summer is considered (i.e., encompassing developing and mature ENSO phases). R^2 indicates the coefficient of determination and *a*, the nonlinear coefficient of the quadratic regression model. Error estimates for R^2 and alpha we calculated as one standard deviation of 1,000 bootstrap realizations. The convection centre index is, by definition, positive for poleward movements of the Convergence Zones referenced at each model's pre-industrial position. Values for each model are presented in Supplementary

Table S1. ~~In panel **d** the dashed line indicates the maximum ENSO variability supported by the climate system (MaxENSO). Maps in this figure were plotted using the cartopy Python library.~~

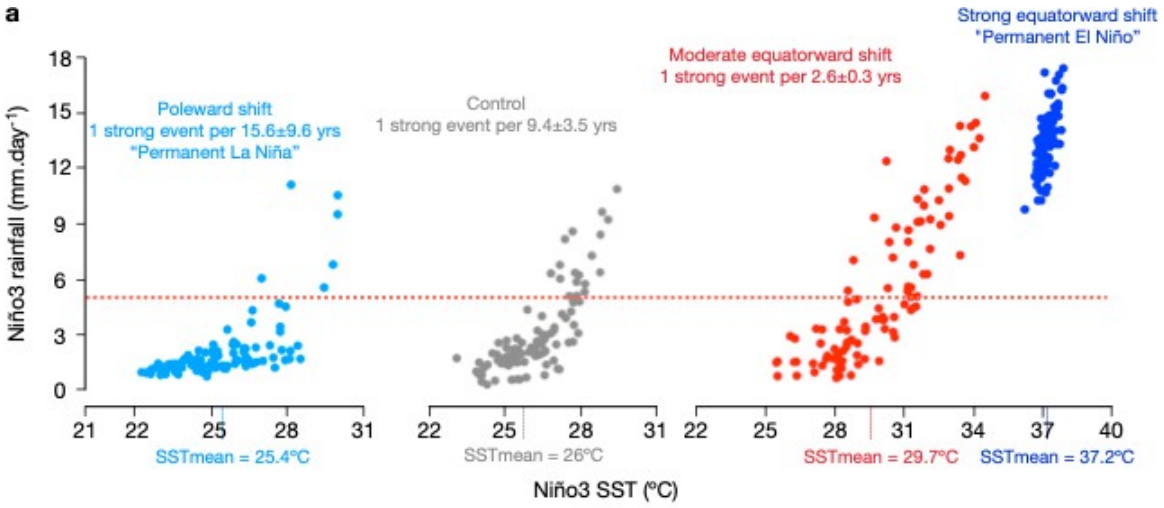
a
Strong equatorward shift
"Permanent El Niño"
Moderate equatorward shift
1 strong event per 2.6±0.3 yrs
Poleward shift
1 strong event per 15.6±9.6 yrs
"Permanent La Niña"
Control
1 strong event per 9.4±3.5 yrs
Niño3 rainfall (mm.day⁻¹)
SSTmean = 25.4°C
SSTmean = 26°C
SSTmean = 29.7°C
SSTmean = 37.2°C
Niño3 SST (°C)

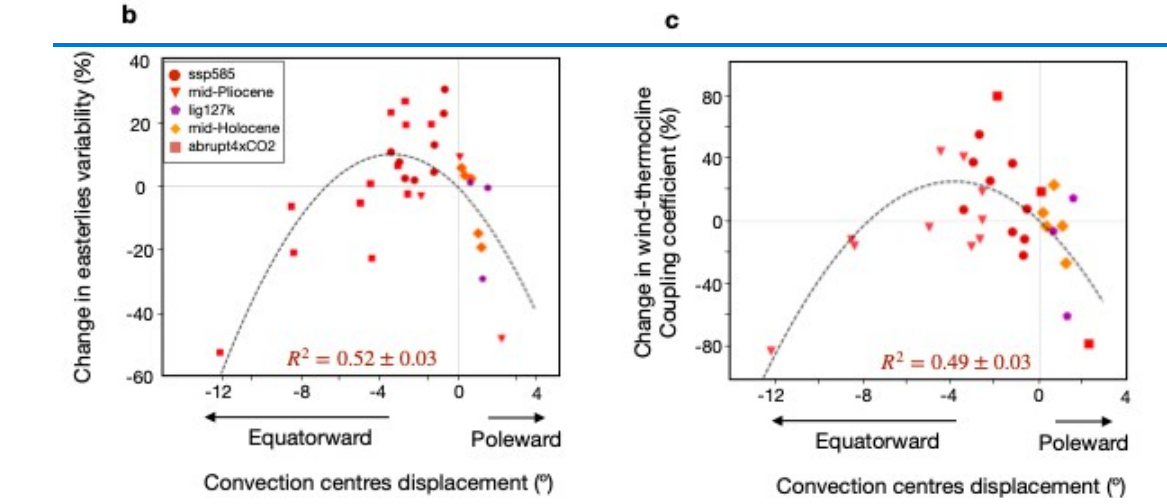
b
c
ssp585
mid-Pliocene
lig127k
mid-Holocene
abrupt4xCO2
Change in easterlies variability (%)
Change in wind-thermocline Coupling coefficient (%)
$R^2 = 0.52 \pm 0.03$
$R^2 = 0.49 \pm 0.03$
Equatorward
Poleward
Convection centres displacement (°)

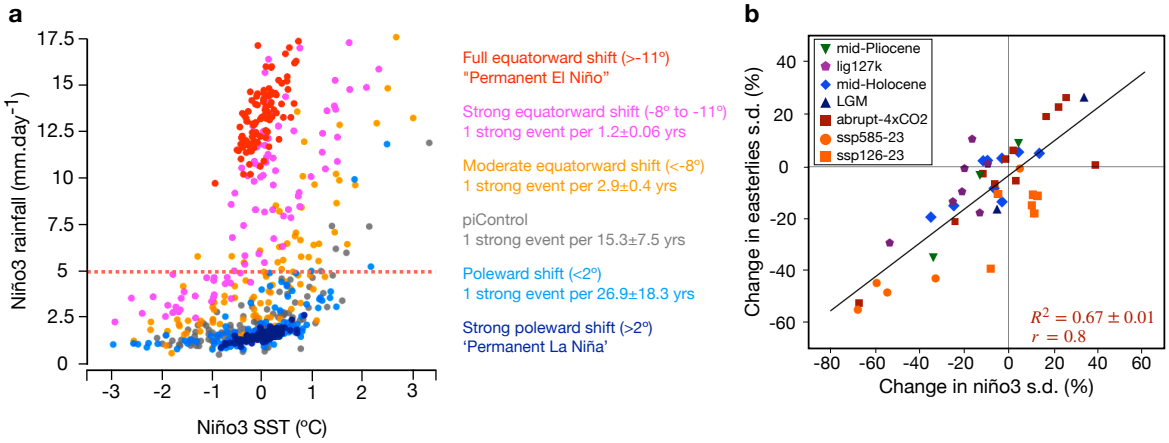
a
Niño3 rainfall (mm.day⁻¹)
Niño3 SST (°C)
Full equatorward shift (>-11°)
"Permanent El Niño"
Strong equatorward shift (-8° to -11°)
1 strong event per 1.2±0.06 yrs
Moderate equatorward shift (<-8°)
1 strong event per 2.9±0.4 yrs
piControl
1 strong event per 15.3±7.5 yrs
Poleward shift (<2°)
1 strong event per 26.9±18.3 yrs
Strong poleward shift (>2°)
'Permanent La Niña'
b
mid-Pliocene
lig127k
mid-Holocene
LGM
abrupt-4xCO2
ssp585-23
ssp126-23
Change in easterlies s.d. (%)
$R^2 = 0.67 \pm 0.01$
$r = 0.8$
Change in niño3 s.d. (%)

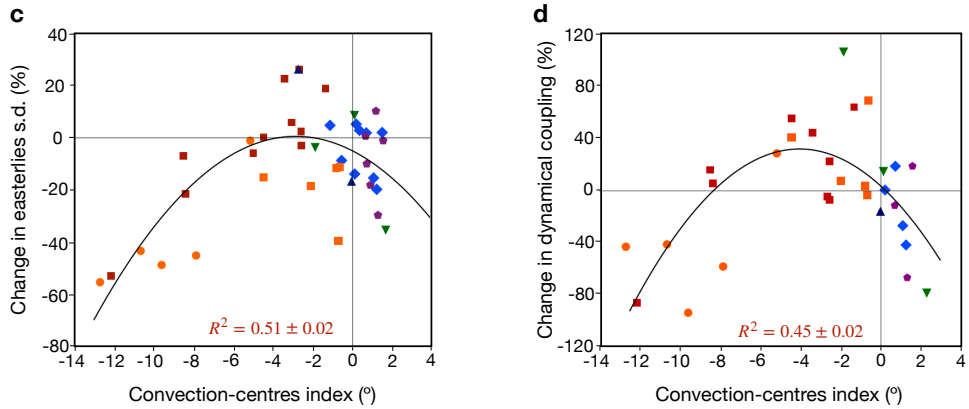
c
d
Change in easterlies s.d. (%)
Change in dynamical coupling (%)
$R^2 = 0.51 \pm 0.02$
$R^2 = 0.45 \pm 0.02$
Convection-centres index (°)

Fig. 3. Equatorial Pacific climate and ENSO feedbacks. a Nonlinear convective feedback: relationship between DJF Niño3 SSTs and DJF Niño3 rainfall. The first 100 years of 1,000 bootstrap realization is shown to illustrate the relationship in each group: pre-industrial control, moderate equatorward (-8º<D<0º), strong equatorward (-12º<D<-8º), full equatorward (D<-12º), poleward (D>0º) and strong poleward (represented by CCSM4-UTRECTH mid-Pliocene simulation) displacements. ~~Models were grouped into 3 subgroups according to the magnitude of the shift of the convection centers: poleward (>0º), and moderate (<9º) or strong (>9º) equatorward displacements. The 1000 samples of 100 years were obtained through the bootstrap method (Methods). The plot shows the first 100-years sample of each group.~~ The frequency of extreme events is indicated by the mean frequency of events that exceeded 5 mm ~~.~~day^{-1} across all realizations (orange dashed line). Error estimates are indicated by the standard deviation of the realizations. **b** inter-model relationship between the change in niño3 amplitude and the change in easterly winds variability in the western equatorial Pacific (5ºS-5ºN; 160ºE-210ºE). **c~~b~~** inter-model relationship between the ~~displacement of the~~ convection~~ ~~centers index and change in easterly wind~~s~~ variability. **~~c~~ d** inter- model relationship between the ~~displacement of the~~ convection~~ ~~centers index and the wind~~ ~~thermocline coupling coefficient. R^2 indicates the coefficient of determination of the quadratic regression model. Error estimates are given by the standard deviation of 1000 bootstrap realizations.

Results shown in this figure were obtained through analyses of the subset models that best simulate the equatorial nonlinear convective feedback (Supplementary Table S1).

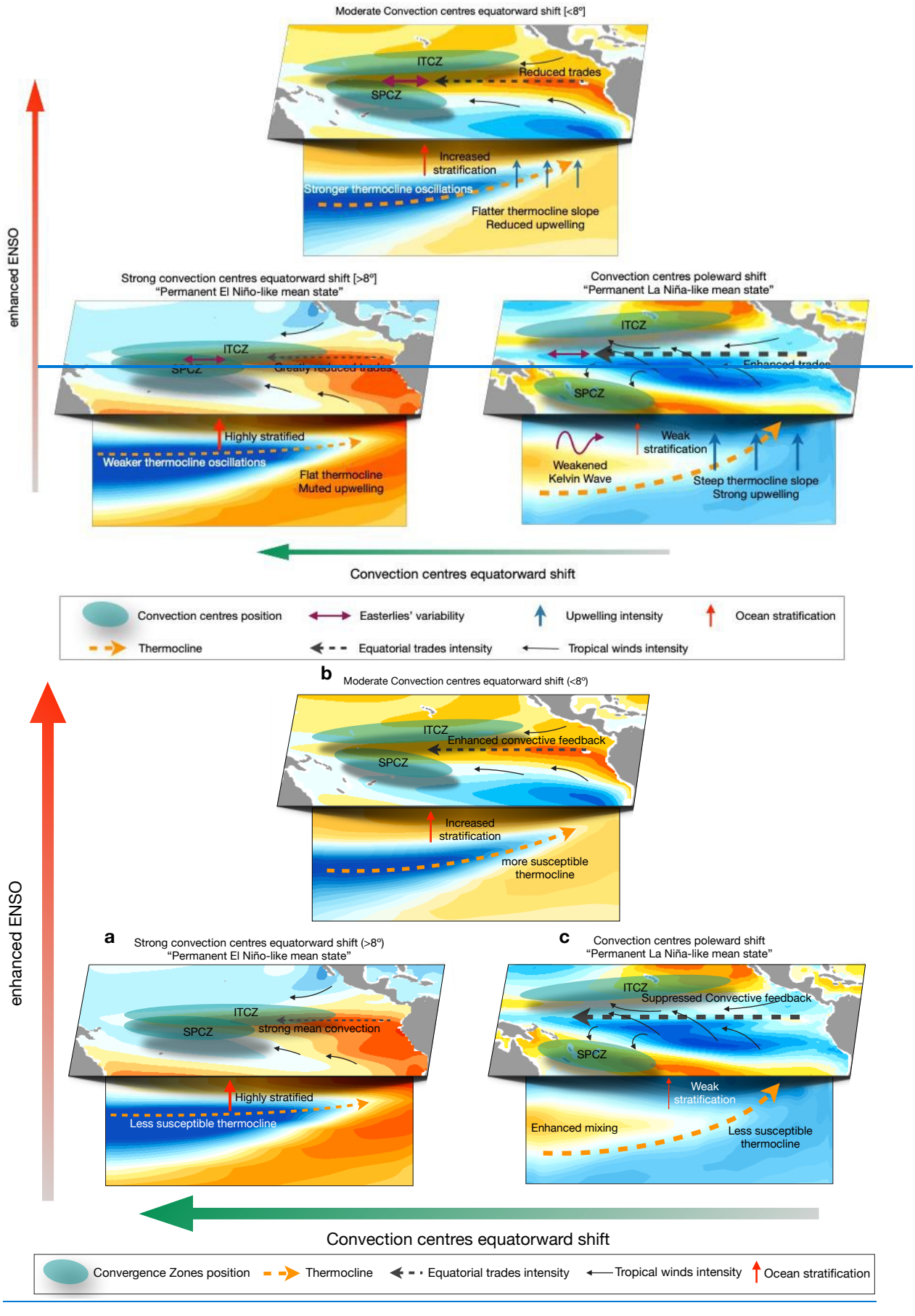
Moderate Convection centres equatorward shift [<8°]
ITCZ
Reduced trades
SPCZ
Increased stratification
Stronger thermocline oscillations
Flatter thermocline slope
Reduced upwelling
enhanced ENSO
Strong convection centres equatorward shift [>8°]
"Permanent El Niño-like mean state"
ITCZ
Highly stratified
Weaker thermocline oscillations
Flat thermocline
Muted upwelling
Convection centres poleward shift
"Permanent La Niña-like mean state"
ITCZ
SPCZ
Weak stratification
Weakened Kelvin Wave
Steep thermocline slope
Strong upwelling
Convection centres equatorward shift
Convection centres position
Easterlies' variability
Upwelling intensity
Ocean stratification
Thermocline
Equatorial trades intensity
Tropical winds intensity
b
Moderate Convection centres equatorward shift (<8°)
ITCZ
Enhanced convective feedback
SPCZ
Increased stratification
more susceptible thermocline
enhanced ENSO
a
Strong convection centres equatorward shift (>8°)
"Permanent El Niño-like mean state"
ITCZ
SPCZ
strong mean convection
Highly stratified
Less susceptible thermocline
c
Convection centres poleward shift
"Permanent La Niña-like mean state"
ITCZ
Suppressed Convective feedback
SPCZ
Weak stratification
Enhanced mixing
Less susceptible thermocline
Convection centres equatorward shift
Convergence Zones position
Thermocline
Equatorial trades intensity
Tropical winds intensity
Ocean stratification

Figure 4 | Mechanisms for changes in ENSO activity across climate states. Schematic of mean state features associated with ENSO variability. **a** full equatorward shift of the convection centers results in flat thermocline, highly stratified upper-ocean and weak dynamical coupling, thus reducing ENSO activity. **b** moderate equatorward shift of the convection centers weakens the equatorial coupled circulation and increases the dynamical coupling, increasing thermocline swings and ENSO variability. **c** poleward shift of convection centers enhances equatorial coupled circulation and reduces the dynamical coupling and ENSO activity. All comparison statements are relative to the pre-industrial climate. ~~Bottom right: A poleward shift of convection centers enhances equatorial coupled circulation and reduces the dynamical coupling and ENSO activity. Bottom left: A full equatorward shift of the convection centers results in a very weak coupled circulation, flat thermocline, a highly stratified upper-ocean and weak dynamical coupling, thus reducing ENSO activity. Top: A small equatorward shift of the convection centers decreases equatorial coupled circulation and increases kelvin wave energy, increasing thermocline swings and ENSO variability. All comparison statements are related to the pre-industrial period.~~ Maps in this figure were plotted using the cartopy Python library.

Appendix ~~A~~

~~The model's ability to simulate the nonlinear Bjerknes feedback is assessed through the nonlinear relationship between the first two principal components of monthly SST anomalies in the tropical Pacific. Models were required to simulate the parameter a, given by the nonlinear coefficient of the fitted quadratic model, greater than half of the observed value (a_{obs}=0.32, Supporting Information Fig. S3) (Takahashi et al., 2011). The criteria used to select model that correctly capture the strength of the convective feedback is based on an essential definitionof extreme ENSO-related rainfall events, which are defined as precipitation events greater than 5 mm/day^{-1} in the Niño3 region. In observations, the 5 mm/day^{-1} rainfall rate is achieved at an SST anomaly of 2ºC, which gives a convective feedback of 2.5 mm/day^{-1}/ºC^{-1} (SupportingInformation Fig. S2). To ensure that models capture the observed strength, models were required to simulate convective feedback greater than 2 mm.day^{-1}.ºC^{-1} in their pre-industrial runs. The model's ability to properly simulate ENSO skewness filters out models that systematically simulate overly wet (i.e., double ITCZs) and dry conditions (i.e., overly strong cold tongue) in the eastern equatorial Pacific. These models simulate SSTs well below or above the convective threshold of 26-28ºC (Johnson & Xie, 2010), thus simulating unrealistic convective feedback.~~

~~The maximum precipitation regions are used as a proxy of the meridional positions of the ITCZ and SPCZ. The ITCZ position is taken as the average latitudes over which precipitation in the tropical North Pacific Ocean (0º-20ºN) is greater than 50% of the maximum zonally averaged precipitation over 120ºE-90ºW. The position of the SPCZ is obtained in a similar way but considering the tropical South Pacific (20ºS-0º). This methodology captures migrations of ITCZ and the SPCZ independently from one another. Given that our objective is to quantify their overall displacement with respect to the equator, this is calculated as their absolute shift:~~

$$D = [|ITCZ_S| - |ITCZ_{PI}|] + [|SPCZ_S| - |SPCZ_{PI}|]$$

~~where the subscript 'S' denotes paleo (mid-Pliocene, LIG, LGM or mid-Holocene) or projection (ssp585) scenarios, while the subscript 'PI' denotes the pre-industrial simulation used as reference. A negative (positive) displacement (D) indicates an overall equatorward (poleward) shift. It is important noting that double-ITCZ biases may affect the SPCZ position. The double-ITCZ bias is an artificial feature produced by most climate models that overestimates the tropical precipitation south of the equator in the central-eastern Pacific.~~

Appendix Text A1

The criteria used to select models that correctly capture the strength of the convective feedback is based on an essential definition of extreme ENSO-related rainfall events, which are defined as precipitation events greater than 5 mm day^{-1} in the Niño3 region. In observations, the 5 mm day^{-1} rainfall rate is achieved at an SST anomaly of 2ºC, which gives a convective feedback of 2.5 mm/day^{-1}/ºC^{-1} (Fig. A1 and Table A1). To ensure that models capture the observed strength, they are required to simulate convective feedback greater than 2 mm.day^{-1}.ºC^{-1} in their pre-industrial runs. Models that do not correctly simulate this feedback tend to simulate SSTs well below or above the convective threshold of 26-28ºC (Johnson and Xie, 2010), resulting in unrealistic convective feedback strength. The model's ability to properly simulate the convective skewness filters out models that systematically simulate overly wet (i.e., double-ITCZs) and dry conditions (i.e., overly strong cold tongue) in the eastern equatorial Pacific.

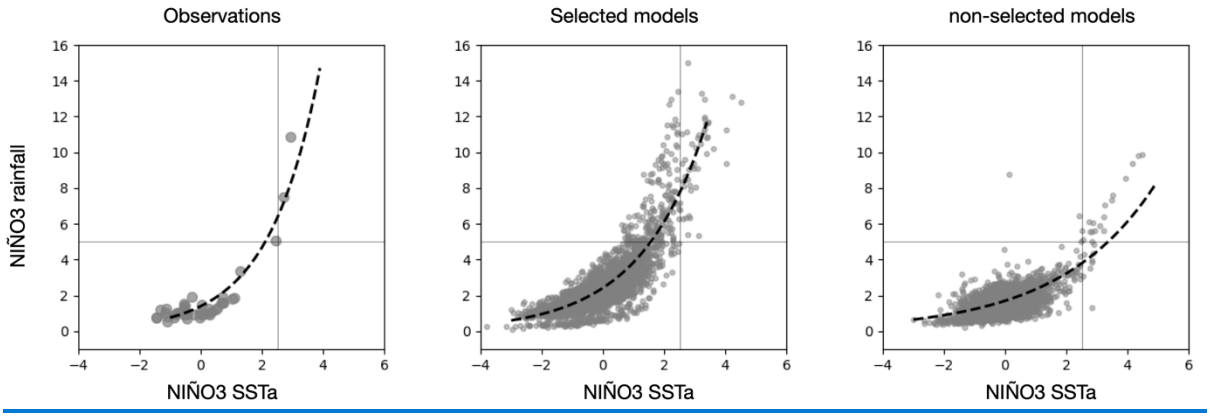

Appendix Fig. A1 – Model selection criteria: convective feedback. Relationship between DJF Niño3 SST anomalies and DJF Niño3 rainfall in observations, selected models and non-selected models. The nonlinear convective criterium is used to select models for the analyses shown in the main manuscript Figs. 2 and 3.

Appendix Text A2

To evaluate the transient response of ENSO activity to the position of the Convergence Zones during the 21st century, we use the SSP3-7.0 scenario. As here we compare ENSO variability with the climatological position of the Convergence Zones, this scenario shows a less intense transient forcing than the SSP5-8.5, thus potentially making this comparison less inaccurate. To reduce this uncertainty we use the time-slice from 2051 to 2100. Results show that the climatological position of the Convergence Zones also modulates ENSO activity during a transient warming (Fig. A2). Future anthropogenic warming under the SSP3-7.0 scenario tends to displace the convection centers equatorward by up to 4.2º, lying in the group of 'enhanced ENSO activity'. Consistently, all but one model simulate increased ENSO activity in the second half of the 21st century under the SSP3-7.0 scenario (Fig. A2).

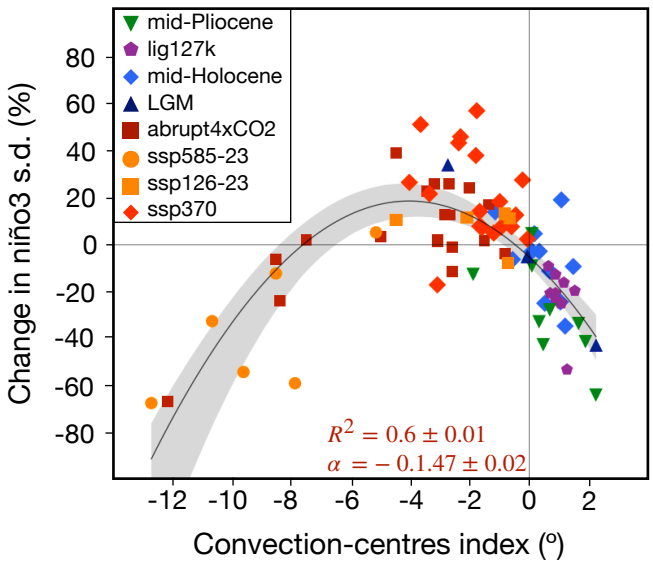

Appendix Fig. A2 – Relationship between changes in ENSO variability and the convection-centers index. Solid black line indicates the quadratic fit based on the least squares method. Banding indicates 95% confidence interval based on a 1,000-sample bootstrap. R^2 indicates the coefficient of determination and *a,* the nonlinear coefficient of the quadratic regression model. Error estimates for R^2 and alpha are calculated as one standard deviation based on 1,000 bootstrap realizations.

To account for ENSO complexity, we evaluate the central (CP) and eastern Pacific (EP) ENSO types (Takahashi et al., 2011), which have distinct anomalies centers in the equatorial Pacific and distinct impacts on remote areas. CP-ENSO variability is characterized by low intensity warming in the central-western Pacific, while EP-ENSO events are recognized by strong warming in the eastern Pacific. CP and EP types are distinguished by the degree of nonlinearity of SST advection from western to eastern Pacific, where enhanced nonlinearity leads to development of intense SST anomalies in the eastern Pacific, associated with EP events. Given this complexity, not all models are able to correctly simulate the two ENSO types due to weak nonlinear SST advection feedback (Takahashi et al., 2011). For this reason, in assessing the response of the CP and EP to the position of the Convergence Zones, in addition to applying the nonlinear convective feedback criterium for model selection, we also require models to be able to simulate the nonlinear SST advection feedback, known as 'Bjerknes feedback'. The model's ability to simulate the Bjerknes feedback is assessed through the nonlinear relationship between the first two principal components of monthly SST anomalies in the tropical Pacific. Models are

required to simulate the parameter *a*, given by the nonlinear coefficient of the fitted quadratic model, at greater than half of the observed value (a_{obs}=0.32, Fig. A3).

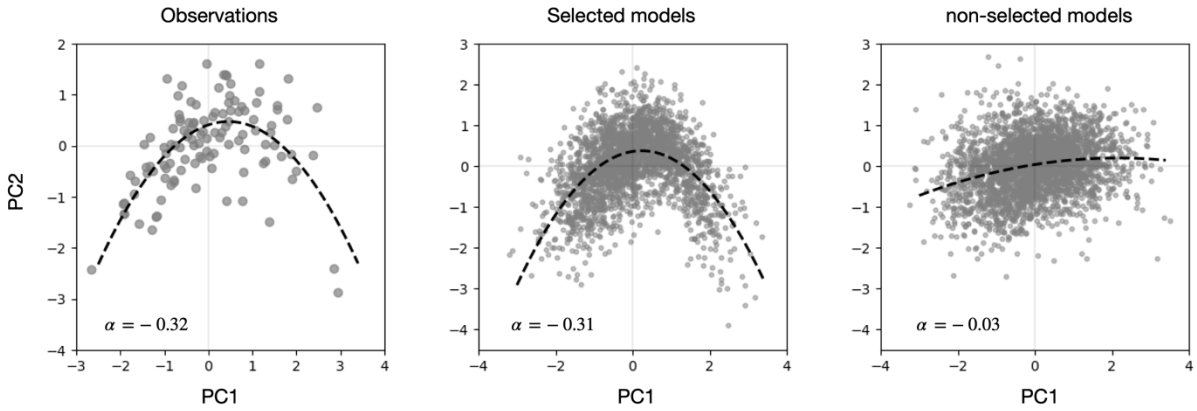

Appendix Fig. A3 – Model selection criteria evaluation: Bjerknes feedback. Relationship between the first and second principal components of SST anomalies in the tropical Pacific in observation (left), selected (middle) and non-selected (right) models. The nonlinear coefficient of the quadratic fitted model is indicated by *a*.

As here we evaluate ENSO dynamics in climate models, the simulated anomaly centers of CP and EP-ENSO may vary across models. As such, indices for CP-ENSO (C-index) and EP-ENSO (E-index) were computed through combining the first two Empirical Orthogonal Functions of SST anomalies in tropical Pacific (15ºS-15ºN; 140ºE-80ºW). The first two principal components time series are combined to obtain the E ((PC1-PC2)/$\sqrt{2}$) and C ((PC1+PC2)/$\sqrt{2}$) indices. The standard deviation of the principal component time series of both C- and E-indices are used as a proxy of their amplitudes.

The relationship between ENSO amplitude change and the displacement of the convection centers reveals important differences between CP- and EP-ENSO types. First, CP-ENSO activity is likely less sensitive to changes in the mean state as indicated by a wider shape of the quadratic fit (Fig. A4a; *a*=-0.79) and weaker relationship (R^2 = 0.33) compared to EP-ENSO (Fig. A4b; *a* = -2.31; R^2 = 0.78). EP-ENSO is strongly modulated by the position of the convection centers (R^2 = 0.75) and exhibits a high nonlinear sensitivity to climate states (a = -2.18; Fig. A4b). According to this finding, the climate system supports a maximum increase in EP-ENSO variance of approximately 55%, which is achieved with an overall equatorward

displacement in the position of the convection centers of ~4.7º (Figure 2b). It is important noting that the niño3 index likely captures a combination of CP and EP-ENSO variabilities, as its region encompasses both CP and EP anomalies (Takahashi et al., 2011).

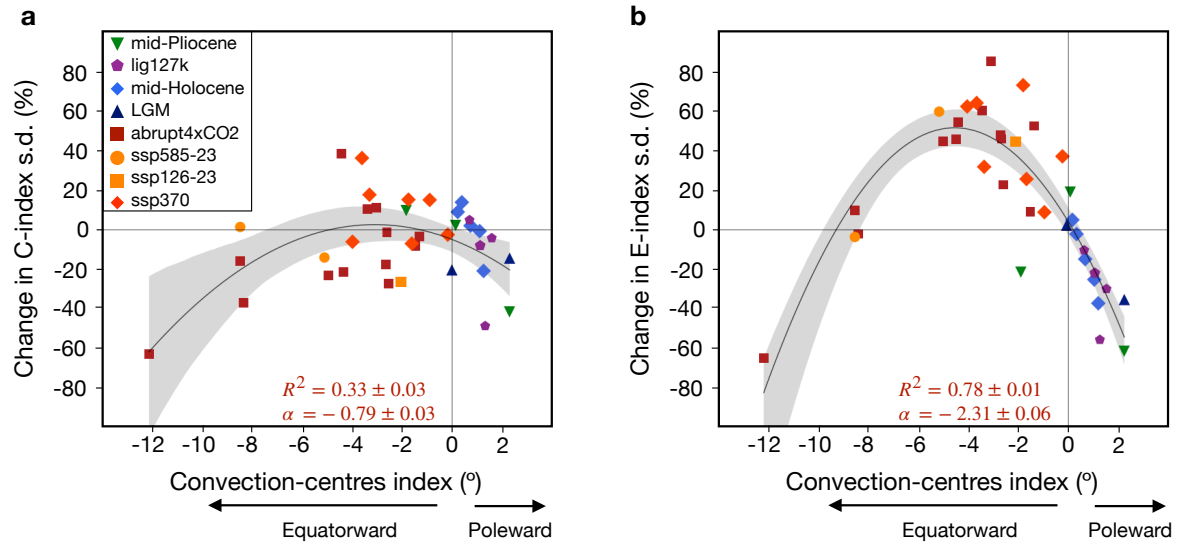

Appendix Fig. A4 – Relationship between C- (a) and E-indices (b) and the convection-centers index. The solid black line indicates the quadratic fit based on the least squares method. Banding indicates 95% confidence interval based on 1,000 bootstrap realizations. R^2 indicates the coefficient of determination, *a* is the nonlinear coefficient of the quadratic regression model. Error estimates for R^2 and *a* were calculated as one standard deviation of 1,000 bootstrap realizations.

Appendix Text A3

The efficiency of the dynamical coupling between the ocean and the atmosphere is measured through the intensity of the wind-thermocline coupling coefficient (Jin et al., 2006). This coefficient measures the sensitivity of the tilt mode of thermocline slope anomalies to wind stress anomalies, which during El Niño events results in eastward temperature advection by downwelling equatorial Kelvin waves:

$$\langle h \rangle_E - \langle h \rangle_W = \beta_h \langle \tau_x \rangle$$

where *h* indicates the thermocline depth, b_h the wind-thermocline coupling coefficient and t_x the zonal wind stress. Subscripts 'E' and 'W' denotes area average in the eastern (5ºS-5ºN; 150ºW-90ºW) and western (5ºS-5ºN; 160ºE-150ºW) equatorial Pacific, respectively. The thermocline depth is computed from the mean temperature profile in each of the boxes

indicated above. This is the weighted average depth, based on depths in which the temperature gradients are greater than 750% of its maximum (Pontes et al., 2022). The wind-thermocline coefficient is computed from monthly anomalies, which capture the evolution of the thermocline slope within each single ENSO event.

Appendix B

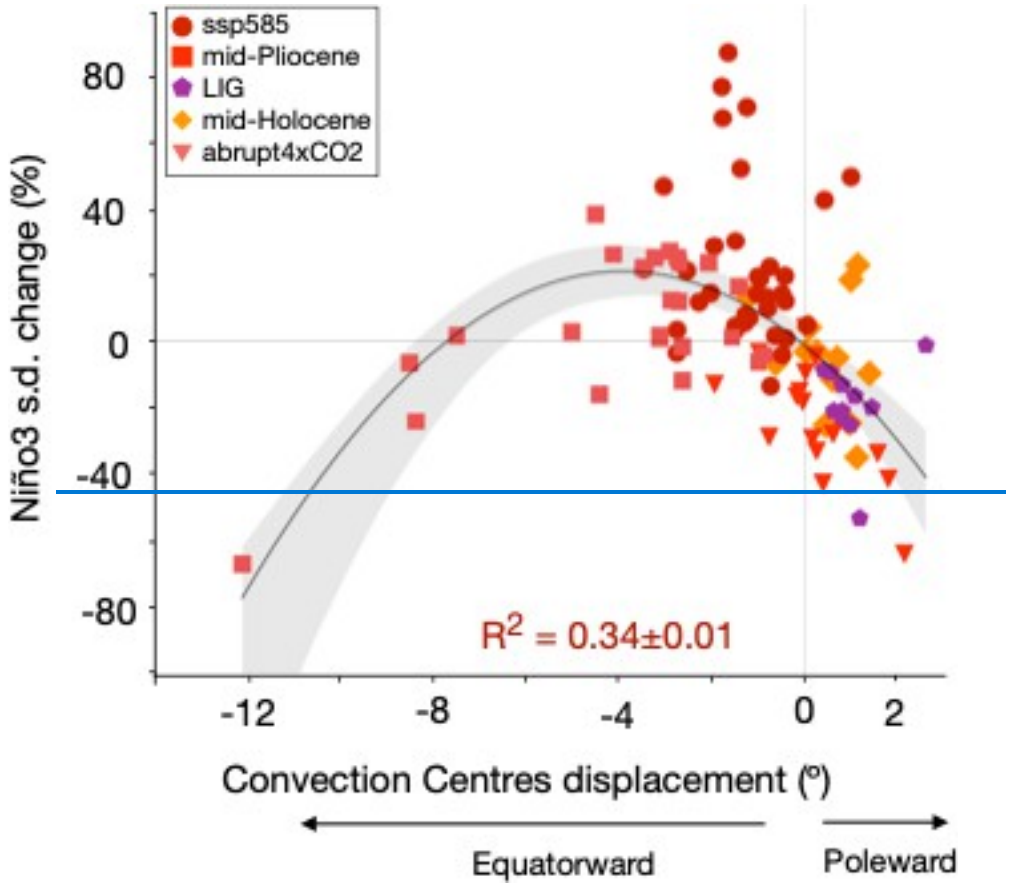

Appendix B Fig. 1B. ENSO-convection centers relationship. Dispersion diagram between the overall displacement in the meridional position of the ITCZ and SPCZ and the Niño3 index. The solid black line indicates the best quadratic fit based on the least squares method. Banding indicates 95% confidence interval based on a 1000-sample bootstrap. The mean displacement of the convection centers boreal spring-summer is considered (i.e., encompassing developing and mature ENSO phases). R^2 indicates the coefficient of determination and a the nonlinear coefficient of the quadratic regression model. Error estimates for R^2 and alpha we calculated as one standard deviation of 1000 bootstrap realizations. No model selection criteria were applied.